Energy Storage Applications of Ionic Redox Transistor Membranes

An Undergraduate Honors Thesis

Submitted to the Department of Mechanical Engineering

Of The Ohio State University

In Partial Fulfillment of the Requirements

For Graduation with Distinction in Mechanical Engineering

Chris Marino

May, 2017

Abstract

Electric vehicles in recent years have offered a cleaner alternative to internal combustion engines (ICE's), but the lithium-ion batteries which power them currently lack the high energy density that gasoline provides. Modern battery architectures like redox flow batteries have achieved higher energy densities than conventional Li-ion batteries, but struggle with capacity fade due to self-discharge across the microporous membranes used to separate the anodic and cathodic cells of the battery. The purpose of this research is to demonstrate the use of an ionic redox transistor membrane, which assumes the function of the standard, porous membrane, and verify its ability to control ion transport between electrodes in a super-capacitor. The smart membrane controls transmembrane ion transport as function of its redox state, which can be adjusted by applying a voltage potential across the membrane. While previous testing of this membrane has primarily been done on small-scale membrane samples, this thesis investigates its function in semi-aqueous electrolyte, scalability of fabrication methods, and its applications in super-capacitor and redox flow batteries. The reduction in equilibration offered by this membrane would facilitate development of redox transistor batteries.

Acknowledgements

I wish to thank Professor Vishnu Sundaresan both for his role in pairing me with this project and his oversight as I worked towards my objectives. He provided me with a great wealth of information at the onset of this work, and is solely responsible for planting the idea of pursuing a research project in my mind.

My sincere thanks go to Travis Hery, for countless hours spent mentoring me in the lab and helping me better my understanding of critical electrochemical concepts. Travis was always willing to provide me with answers to the many questions I had, and even took time away from other pursuits to help troubleshoot, guide, and recommend methods. His knowledge and prior work was a valuable resource to me, and I don't know where my project would have ended up without his efforts.

I would also like to thank Dr. Rob Siston for his part in helping me hone my presentation and offering valuable constructive criticism on my work. Both my speaking skills and the design of my presentation have improved since I started working under his guidance.

Contents

Table of Figures

Chapter 1: Introduction

1.1 Importance of Batteries in Energy Storage

Fueled by volatility in oil prices, climate change concerns, and a need for reliable domestic energy sources, a hastened pursuit of sustainable energy storage materials has gained prominence in recent years. Of the domestic energy sources available, renewables currently hold around a 13% share in total U.S. electricity generation[8], of which roughly half is comprised of hydropower generation. Among these renewables however, intermittent sources of energy such as solar and wind offer the most potential for growth. Projections estimate a two-fold increase in total renewable energy generation over the new two decades[7], comprised mostly of added solar and wind capacity.

As the amount of energy generated by these time- and weather-dependent sources increases, demand for low-cost, reliable methods of energy storage will no doubt grow as well. There currently exists no large-scale energy storage solution for these source types; of current grid-scale storage capacity, hydroelectric energy is most dominant (>99%), but is only feasible on the large scale and has geographic constraints[5,6]. Compressed air energy storage is an option identified specifically for solar power plants, but has low energy density and suffers from the same geometric constraints since compressed air is usually stored in underground caverns[2]. A better solution would entail some type of modular electrical energy storage (EES) system with higher energy density. Several electrochemical EES designs have been proposed to satisfy this need, and will be discussed in a later section.

In addition to grid-scale storage, there exists demand for vehicles with electrified drivetrains and on-board EES systems with both high energy density and specific power. Such a storage system needs to exhibit energy density and specific power comparable to conventional internal combustion engine (ICE) vehicles in order to remain competitive and marketable. The current energy storage landscape (Figure 1) indicates that some types of electrochemical batteries have achieve relative parity in energy density with gasoline engines, but are still about an order of magnitude away in specific power.

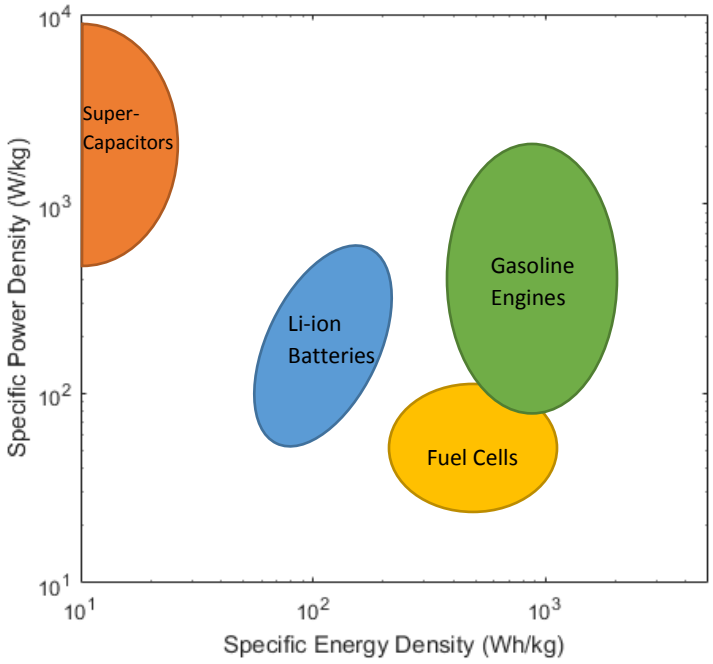

Figure 1: Energy Storage Landscape

Battery chemistries, particularly lithium ion architectures, have been integrated into several electric vehicle (EV) models available on the market today. Limited energy density is not the only downside of electric vehicles; long charging times as illustrated in Figure 2 make

traveling distances farther than 100-200 miles in an EV impossible without stopping to recharge for an extended period of time.

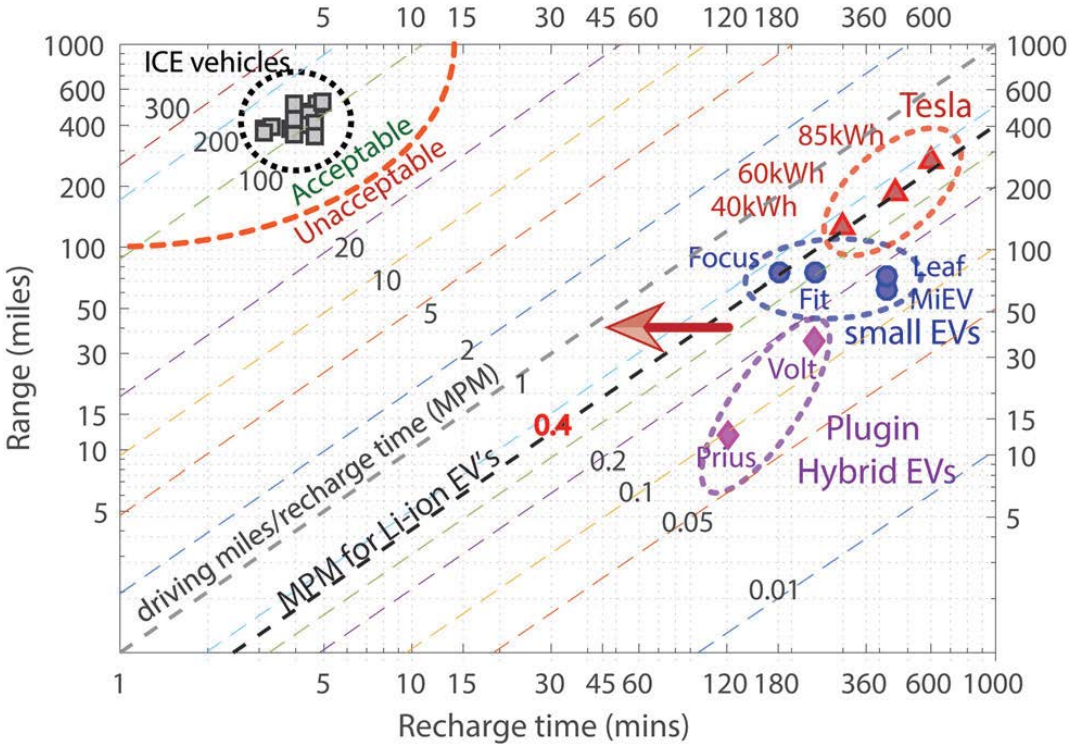

Figure 2: Range vs Recharge Time (Hery, 2016)

Whereas electric vehicles need several hours to charge fully, a depleted gasoline tank can be refilled in just a few minutes, providing hundreds of miles of driving range for only a few minutes of down-time. For electric vehicles to reach performance parity with conventional vehicles, this gap in refuel/recharge time must be diminished.

In this introductory section, we have outlined two markedly different situations where a novel EES solution is needed. Both the grid- and vehicle-level systems discussed above can be improved by utilizing a storage mechanism with increased energy density, while providing the same level of specific power. Applications of such a mechanism would not be limited to these

two scenarios; unmanned aerial vehicles, aviation electronics, and any number of consumer electronics would all be directly impacted by a new generation of modular EES systems.

1.2 Modern Battery Design

Of the recent developments in electrochemical battery architecture, redox flow batteries (RFB's) seem best positioned to satisfy the energy density and specific power requirements previously outlined. In simplest terms, redox flow cells (Figure 3) are comprised of two tanks containing different electroactive solutions and an interfacial chamber connected by piping[6]. The electrolyte solutions are pumped into the interfacial chamber, which is divided into anode and cathode cells by a microporous membrane. Electricity is generated in this chamber as the electrolytes exchange ions across the membrane in a redox reaction. Electrons transferred from these reactions are collected through inert electrodes on either side of the chamber, comprising the output current of the cell.

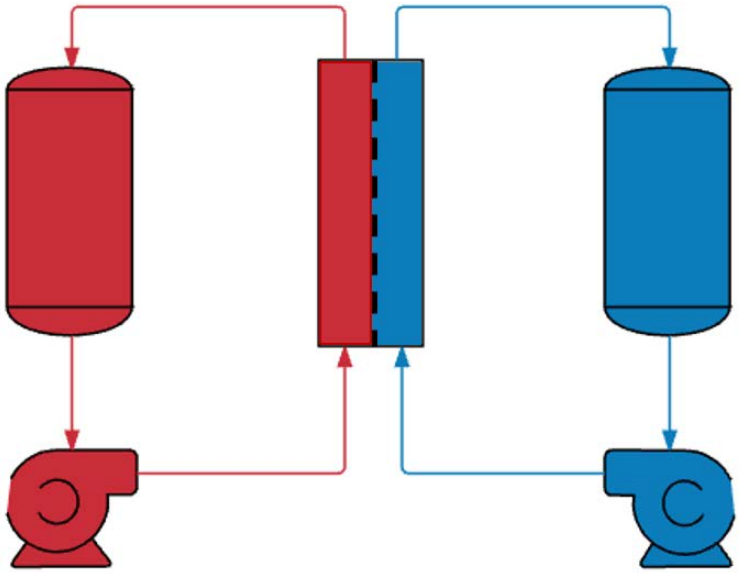

Figure 3: Redox Flow Cell

In this configuration, ion-containing solutions can be selected based on necessary energy density and stored externally from the interfacial flow cell. Electrolyte can be provided whenever necessary, and many flow cells can be connected in parallel or in series to increase power output. While the external storage component of RFB's does not lend itself to small-scale applications, the decoupling of the power and energy characteristics of stacked cells allow for the design of modular systems on medium- to grid-size scales. In addition, there are no geological constraints like those of hydroelectric power or compressed air storage that limit the construction of these redox flow systems. There are, however, some parasitic losses in the system due to the energy required to pump electrolyte into the interfacial chamber, but these losses become less relevant as the system is scaled to larger sizes.

1.3 Limitations of Contemporary Redox Flow Batteries

1.3.1 Electrolyte Composition and Ionic Concentration

As discussed in previous sections, the energy density of a redox flow battery is dependent on the electrolyte, and specifically the amount of ions the electrolyte is capable of containing. For most feasible aqueous redox solutions, this solubility-limited parameter means the concentration of ions dissolved in solution cannot exceed more than 2 M on average[1], which is far below concentrations needed for sufficient energy density. In addition, the dielectric breakdown of water into H_2 and O_2 around -1.2 V limits the range of potentials that can be applied to such a cell. Despite these inherent drawbacks, aqueous solutions are still used in some experiments due to low toxicity and cost. The design space of aqueous electrolytes can be thought of as a proving ground for some battery architectures before scaling up to more energy dense chemistries.

In literature, non-aqueous electrolytes are used more often due to higher concentrations of ion solubility. Alkyl carbonate is one such liquid that offers concentration of lithium ions (from powders such as $LiCoO_2$ and $LiFePO_4$) in the range of 10 to 40 M[1]. These active electrode powders are not dissolved in solution, but rather immersed in the liquid electrolyte as a suspension while still retaining the ability to flow. This configuration is known as a semi-solid flow battery[1], and overcomes typical electrolyte solubility limitations by retaining a solids content around 50-70%.

While retaining high energy density and potential for scaling to high specific power, the electrolyte constituents of this flow battery are far more corrosive than other aqueous

chemistries. Some lithium powders mentioned are also susceptible to thermal-runaway events, a process in which exothermic redox reactions increase the temperature of the electrolyte. This increase in temperature increases the ionic conductivity of the electrolyte, accelerating reaction kinetics which in turn produces heat at a faster rate. This positive thermal feedback is capable of rupturing cells and has been cited as a safety concern in consumer electronics which utilize conventional Li-ion batteries[3]. Though safety architecture exists to shut down thermal events before runaway occurs, the possibility of an incident happening must be taken into account when performing experiments with these more corrosive materials.

1.3.2 Recharge Times

As mentioned in section 1.1, a major drawback of rechargeable batteries, especially those used in electric vehicles, is the slow ion kinetics that require long periods of time to fully recharge depleted batteries. While future advances may improve kinetic rates, it is unlikely that a breakthrough will improve charge time by the two orders of magnitude necessary to become comparable to conventional ICE refuel times. In other words, to achieve charge-time parity with gasoline engines, battery advances must pursue refueling mechanisms over recharging mechanisms.

Redox flow batteries are already well suited to incorporate refueling mechanisms. Unlike conventional lithium ion cells, electrolyte is not restricted within the interfacial chamber, but can flow freely from an external tank whenever necessary. Having undergone redox reactions, the depleted electrolyte can be collected and conventionally recharged later. Once a

cell consumes all electrolyte available from the external tank, refueling simply involves either refilling the external tank or, for grid-scale designs, modifying the piping system such that a valve to a full secondary tank can be opened.

In this manner, electric vehicles fitted with redox flow batteries could swap out battery electrolyte on the order of several minutes instead of several hours. This mechanism could introduce electric vehicles which are able to be filled like gasoline engines and can utilize similar infrastructure that currently exists for refilling conventional vehicles. Electrolyte could be exchanged at locations similar to gas stations, which could then recharge the depleted electrolyte and recycle it for other consumers.

1.3.3 Self-Discharge

In sections 1.3.1 and 1.3.2, we have discussed aspects of redox flow batteries that distinguish their design from conventional lithium-ion architectures. Though markedly different, there are some conventional limitations present in redox flow batteries. One limitation of particular interest to this research is that of self-discharge, or capacity loss of a battery or super-capacitor over time. There are several vehicles of self-discharge that are common in energy storage mechanisms. At capacitive electrode interfaces, where ions form a double layer at the surface of the electrode, electrons have been measured diffusing through the double layer and discharging the capacitor[5]. This diffusion can be reduced by coating the surface in a thin layer of insulating material.

After a double layer has been formed on the electrodes of a capacitor, additional charge accumulates in the region directly behind the layer of ions in electrolyte attracted to the

electrodes. During long periods of charging, this accumulation forms a concentration gradient with high concentrations of ions close to the electrode surface, and less concentration in farther regions of the half-cell. In a large half-cell environment, when the charging potential ceases to be applied to the electrodes, much of this additional charge diffuses into the concentration gradient of the surrounding electrolyte. This loss of charge close to the electrodes is another form of self-discharge, and can be diminished by reducing the area surrounding the electrodes to leave less room for a concentration gradient to build up.

Of self-discharge mechanisms, the vehicle most relevant in the context of redox flow batteries is leakage of ions between one half-cell to another. The anodic and cathodic chambers in a redox flow cell have been mentioned as separated by a microporous membrane, with pores sizes on the order of 0.1 to 10 μm. These membrane separators permit transport of small sized ions (typically cations) from one half-cell to another, but cannot mediate transport under normal operating conditions.

Therefore, if battery electrolyte capable of undergoing redox reactions is placed on either side of such a separator, the cell will undergo those reactions until both electrolytes are depleted. This discharge causes capacity losses if any electrolyte is present in the interfacial chamber while the battery is no longer in use. Similarly, in a capacitive set-up where separating charge between half-cells is necessary, ions will immediately diffuse across the membrane separator once charging potential is no longer present. This particular method of self-discharge is common to all EES mechanisms that employ microporous membranes as half-cell separators.

1.4 Ionic Redox Transistor Membrane

A recent membrane material development may yield a solution to the problem of self-discharge in redox flow cells. In recent literature, a device has been created that can be categorized as a smart membrane separator, and while first developed as a tunable cation sensor[9] has been demonstrated to have applications as an EES component[4].

This separator, denoted as an ionic redox transistor membrane in literature, is comprised of a standard microporous membrane coated with gold onto which a conductive polymer doped with a bulky anion is electropolymerized. The conductive polymer, polypyrrole, formed over the pores of the membrane, ensnares bulky dodecylbenzene sulfonate (DBS) ions while they are attracted to the conductive membrane surface. When the membrane is immersed in an ionic solution, each DBS anion acts a redox site for positively charged cations to enter into the membrane through. Applying a negative potential to the membrane attracts cations, which ingress using these redox sites. These cations, in aqueous solution, have hydration shells composed of several water molecules with dipoles oriented towards the positively charged ion. The ingress of these cations and their hydration shells into the membrane, which causes expansion of its volume and widening of its substrate pores. These mechanistic changes in the membrane aid ion transport in the reduced state.

If a positive potential is applied to the membrane via its conductive surface, cations are repelled away from the polymer as its charge becomes either positive or net neutral. When the bulk of the polymer is positively charged, the trapped DBS anions are attracted to the gold surface, compressing the polymer into a tightly packed state. This state of high packing density

covers up pores in the membrane substrate, restricting ion transport across the membrane separator. Consequently, as the membrane moves from being reduced at negative potentials to oxidized at positive potentials, the rate of transmembrane ion transport is decreased. This ability of the smart membrane to control this transmembrane current based on an applied potential parallels the characteristics of transistors in conventional circuits, and explains the name 'ionic redox transistor membrane'.

The development of the ionic redox transistor membrane offers a potential solution to the self-discharge that has plagued even the most modern designs of batteries and super-capacitors. The capacity to reduce or eliminate leakage current in super-capacitors would have profound applications in EES, specifically in solar power collection where the harvested current is typically smaller than the inherent leakage current in the cell, making energy storage impossible[8]. In batteries, particular redox flow architectures, a smart membrane separator would minimize loss by shutting down redox reactions while the battery is not in use.

1.5 Objectives

Developing better, more efficient methods of harnessing energy hinges on the ability to significantly reduce the amount of self-discharge that occurs in energy storing mechanisms over time. The ionic redox transistor membrane discussed in the previous section is a marked improvement compared to the membrane separator technology that currently exists to serve this purpose.

While several studies such as Hery (2016) have been conducted to determine the characteristics of such membranes in controlling ion transport, no study as of yet has measured

the leakage current that occurs across ionic redox transistor membranes. Furthermore, the sizes of membrane samples used in experiments to date are somewhat small (around 0.3 cm^2). These sample scales are beneficial when testing and evaluating membranes, but no studies have yet incorporated larger sizes of ionic redox transistor membranes to demonstrate their applications to industry and large-scale manufacturability.

Therefore, through experimental electrochemical testing, the purpose of this research is to investigate the effect of the ionic redox transistor membrane on the amount of leakage current that occurs through self-discharging and forced-discharging cells. In addition, it is the objective of this research to explore the design and fabrication of larger membrane sizes in order to demonstrate reliable manufacturing techniques and membrane characteristics.

This thesis contains 4 chapters. Chapter 2 will represent the methods used to gather results for this study, including experimental set-up and procedure. Chapter 3 presents the results and analysis retrieved from the experimental analysis, as well as discussion. Chapter 4 presents a conclusion informed from the discussion in the previous chapter. Included at the end is a bibliography containing all pertinent references in the study.

Chapter 2: Methods

2.1 Introduction

The purpose of this section is to represent the methods and experimental set-up used in the creation of transistor membranes, their characterization, and subsequent testing. The tests

for this research were electrochemical in nature, and involved a series of electrodes immersed in various solutions. For experiments involving 3- and 4-electrode cells, a HEKA ELP3 ElProScan bipotentiostat was used to both apply potentials and measure resulting currents. This section also includes a segment on the types of data correction and post-processing that occurred after running experiments on the bipotentiostat. MATLAB code was used for these operations.

2.2 Membrane Creation

2.2.1 Fabrication of Membrane Electrodes

Standard porous membrane separators were purchased to be used as a substrate for the electropolymerization of polypyrrole doped with dodecylbenzenesufonate (PPy(DBS)). For the testing of small-scale membrane samples, discs were punched from track-etched polycarbonate (PCTE, 600 nm pores, 9.3% porosity), while sheets of Celgard film (25 µm pores, 41% porosity) were cut to size for use in larger membranes. Both types of porous substrate were sputtered with gold to allow the application of the electric field necessary for electropolymerization of conducting polymer onto the membrane. Once sputtered with gold, the resistance of the conductive substrate surface was collected with a voltmeter, and observed to be on the order of 10 Ω. The gold surface was electrically connected with silver wire dipped in silver paste, which was epoxied in place to remove any interference from exposed silver in electrochemical measurements. Average area of the PCTE membrane electrodes created using this method was 0.3 cm^2 (hereafter referred to as 'small membranes'), while the area of the larger Celgard membranes ('large membranes') was around 25 cm^2.

2.2.2 Electropolymerization of Membrane Substrate

Pyrrole (reagent grade, 98%) and sodium dodecylbenzene sulfonate (NaDBS, technical grade) were purchased from Sigma Aldrich. An electropolymerization solution consisting of 0.2 M pyrrole and 0.1 M NaDBS was prepared using deionized water (resistivity 18.2 M Ω.cm). The working membrane electrode (WE) was placed in this solution along with a carbon paper counter electrode (CE) of similar size positioned in parallel with respect to the membrane. An Ag/AgCl pellet reference electrode (RE) was placed in between the working and counter electrodes. An ElProScan ELP3 (HEKA Elektronik Dr Schulze GmbH) bipotentiostat was used to apply an electropolymerization potential of 0.42 V with respect to the reference electrode while observing the amount of charge deposited on the membrane. During this process, called chronoamperometry, pyrrole polymerizes onto the membrane while the negatively charged DBS^- anion is attracted to the membrane surface, resulting in strands of polypyrrole ensnaring DBS^- anions within the polymer attached to the porous substrate. Electropolymerization continues until the total charge accumulated on the membrane, regardless of size, reaches an areal charge density of 1.5 C/cm^2. For the small membranes, the total accumulated charge necessary is around 475 mC. For the large membranes, the total charge necessary is 37.5 C. The thickness of the polymer created using this process is directly proportional to the amount of accumulated charge.

The electropolymerization process is relatively simple for small membrane samples. The 0.3 cm^2 membranes are small enough that the polymerization process can be conducted within a 10 mL beaker with electrode surfaces oriented vertically. However, to translate this setup to the larger membranes would require an extremely large beaker and an inordinate amount of

polymerization solution. To remedy this issue, a polymerization chamber was constructed using several laser-cut layers of acrylic epoxied together (Figure 4).

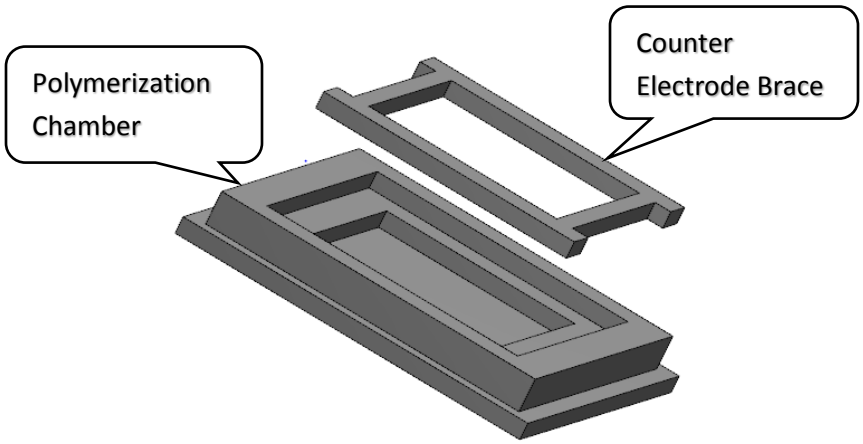

Figure 4: Solid Edge Model of Polymerization Chamber

This chamber allows a working membrane electrode to be placed gold-sputtered side up on the bottom of the chamber (Figure 5), which is then filled with polymerization solution.

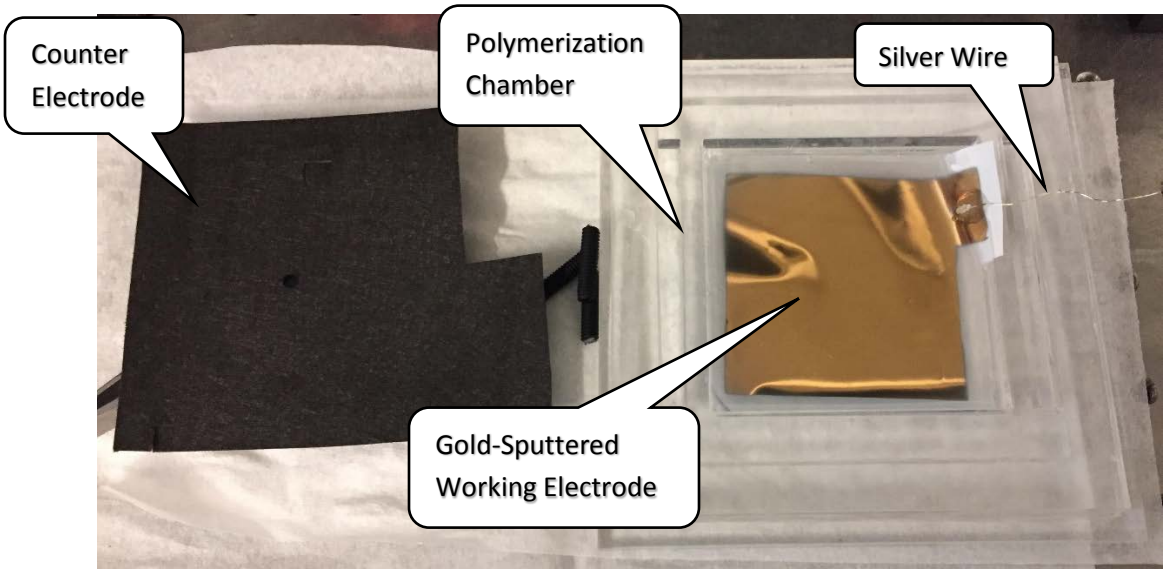

Figure 5: Placement of Working Electrode in Polymerization Chamber

The counter electrode is positioned on top of the lip created by the middle acrylic layer. A fit-in acrylic piece is then placed on top of the counter electrode to fix it in place and prevent excessive sagging once the electrode becomes wetted. A small hole is punched in the middle of the counter electrode to allow an Ag/AgCl pellet electrode to be suspended between the counter and working electrodes as a reference. This setup allows for ideal, repeatable polymerization conditions, as the separation between the CE and WE is around 0.5 cm, similar to conditions created in the beaker at small membrane scales. In addition, the horizontal orientation of this chamber requires a minimal amount of polymerization solution (~16 mL) to be used for each membrane. Figure 6 shows the chamber fully assembled and ready for electropolymerization.

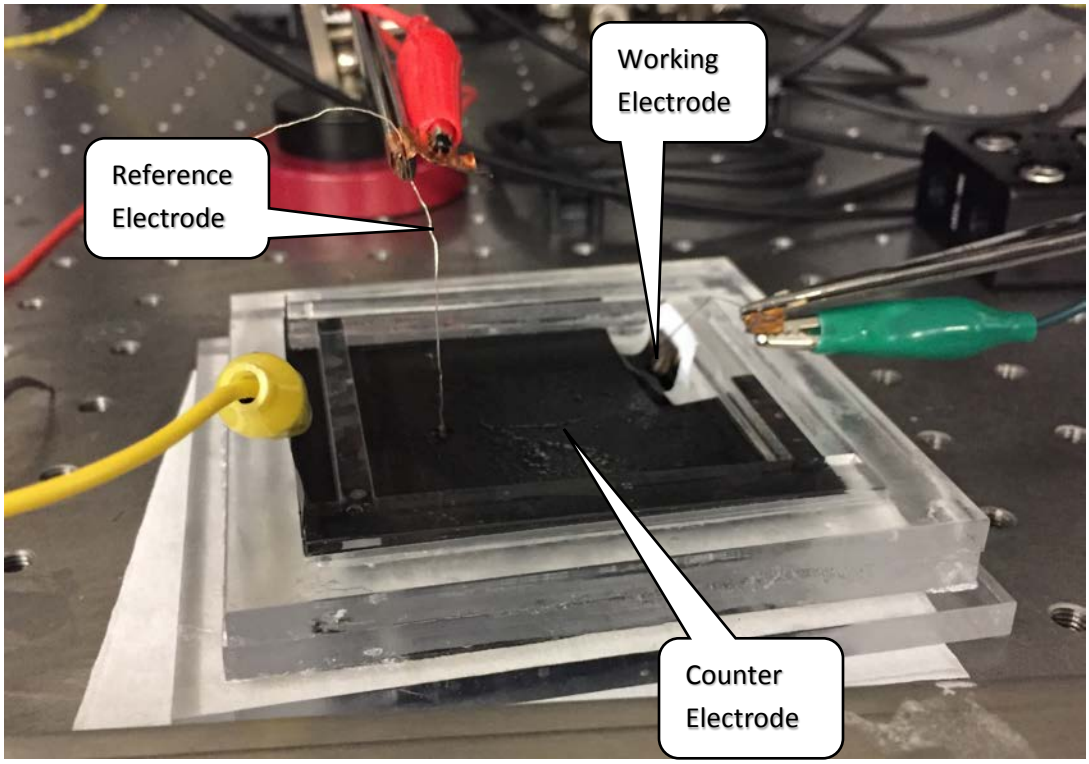

Figure 6: Fully Assembled Polymerization Chamber

2.3 Membrane Characterization and Testing

2.3.1 Membrane Characterization through Open Cell CV

After electropolymerization, the membrane is removed from the chamber, rinsed with deionized water (DI), and dried under an N_2 stream. At this point, the polymerization process has finished and DBS^- ions are successfully ensnared in the polymer. PPy(DBs) spans the pores of the substrate, and forms a physical barrier against ion transport, but no pathways have been created in the bulk of the polymer for ions to move through. Characterization and formation of the qualities that constitute the newly created ionic redox transistor membrane are accomplished by varying the potential applied to the membrane at a set rate while it is immersed in a cation containing solution. This process, known as cyclic voltammetry, is crucial in understanding the ion transport behavior of the membrane as its redox state is altered.

An electrolyte solution is created containing 0.8 M potassium gluconate dissolved in a 50/50 mix of DI water and ethylene glycol. Potassium gluconate was chosen as an electrolyte due to its bulky gluconate anions and its solubility in semi-aqueous solution. For small membrane electrodes, the setup again involves immersing the membrane in a 10 mL beaker containing the electrolyte solution, with the CE and RE positioned in the same configuration as they were in the electropolymerization setup. For large membranes, the polymerization cell setup is used in the same fashion, with the only difference being the usage of electrolyte solution. The membrane is rinsed in DI water and dried with an N_2 stream before immersion.

Once the cell is fully assembled, an ElProScan ELP3 bipotentiostat was used to cycle the voltage potential applied to the membrane at a set rate, while monitoring the resulting current. As the potential becomes more negative, the bulk of the polymer becomes more negatively charged, and cations in solution are drawn into the polymer during this reduced redox state. As the potential becomes more positive, the bulk of the polymer becomes electroneutral due to the presence of trapped DBS^- anions. In this oxidized redox state, cations in solution balance the electroneutrality by either entering or exiting the polymer. At highly positive potentials, cation movement is dominated by egress out of the polymer.

The voltage range was altered slightly for each membrane in order to capture the potentials at which the maximum rate of ions entering or exiting the polymer occurred. For small membranes, this potential range was generally around -1.1 to 0.3 V; in large membranes, -1.6 to 0.5 V. Applied potential very rarely exceeds these ranges, as more negative potentials will begin dielectric breakdown of the water present in solution, and more positive potentials will over-oxidize the polypyrrole in the membrane, causing irreparable damage. Scan rates for these open cell CV's were consistently 50 mV/s.

Several cycles of cyclic voltammetry were necessary for membranes to reach an equilibrium state. The first few CV cycles after electropolymerization do not exhibit consistent current responses as the cations are creating new pathways into and out of the bulk of the polymer. After 20-30 cycles, the current response reaches an equilibrium where the behavior is consistent from cycle to cycle. Once this equilibrium is reached, the membrane is removed from solution, rinsed with DI water and dried under an N_2 stream, then stored in a petri dish between

tests. Samples of the small and large scale membranes are shown in Figures 9a and 9b respectively.

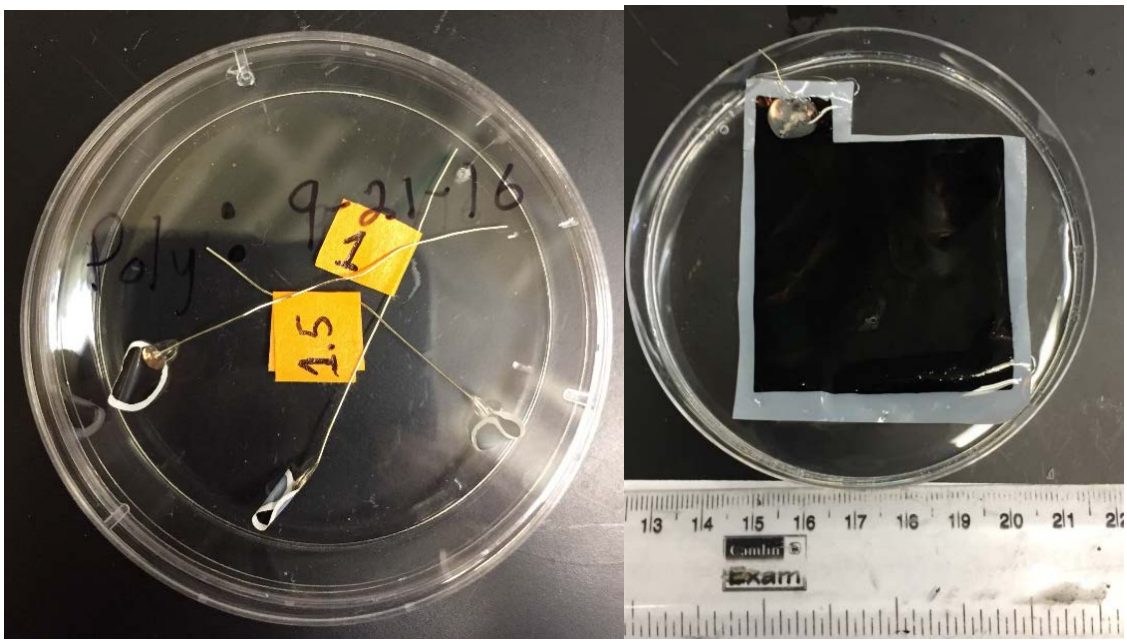

Figure 7a and 9b: Small Scale Ionic Redox Transistor Membranes

2.3.2 Small Scale Closed Cell Setup and Preparation

Once a membrane has been equilibrated and characterized using CV, it will exhibit consistent behavior in further testing. Testing in a “closed cell”, or a chamber in which the membrane separates two half-cells of electrolyte in a super-capacitive set-up, is done directly after characterization to determine the ability of the membrane to transport ions between half-cells in a controlled manner. For small membranes, an existing Delrin™ chamber (Figure 8) was used for closed cell testing.

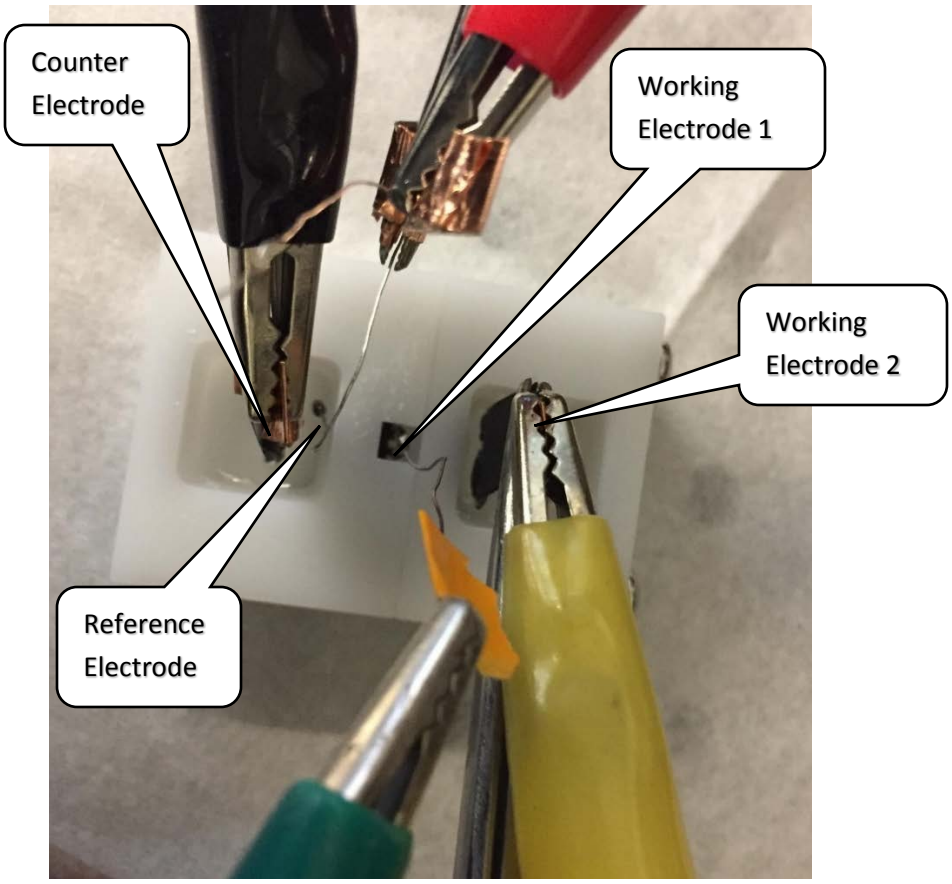

Figure 8: Small Closed Cell Chamber

The membrane was placed in between the half-cells, face down on an O-ring to ensure a water-tight seal. An Ag/AgCl reference electrode was placed in one half-cell, along with a strip of carbon paper acting as the counter electrode, which acts as the cathode during charging intervals. A second carbon paper electrode was placed in the other half-cell, acting as the second working electrode, and anode during charging intervals. While the membrane working electrode controls the ion transport across the cell, the second working electrode applies a potential between itself and the counter electrode, constituting the driving potential that either charges or discharges the cell based on its value.

The half-cell with the reference electrode was filled with an electrolyte solution of 0.8 M potassium gluconate dissolved in a 50/50 mix of DI water and ethylene glycol by volume. The half-cell with the second working electrode was filled only with a 50/50 mix of DI water and ethylene glycol. The differences in cell electrolyte composition make for an easier analysis of charge storage and ion transport conditions. Since gluconate is a large bulky anion, it cannot pass through the small pores in the membrane substrate. Because of this condition, if potassium gluconate were present on both sides of the chamber, the bulky gluconate ions could not cross over to the positively charged cathode during charging, and would interfere with attributing charge measurement in the anodic cell to potassium ions. Placing potassium gluconate on only one side of the chamber allows for a fully charged cell containing only gluconate on one side, and only potassium on the other, greatly simplifying the analysis of leakage current and charge storage in the cell.

2.3.3 Large Scale Closed Cell Setup and Preparation

For large membranes, a similar setup is used involving potassium gluconate on one side of the chamber only. The general 4-electrode architecture remains consistent between both cells, but the large-scale super-capacitor setup is decidedly more complex. A Proton Exchange Membrane Fuel Cell kit was purchased from H-TEC Education, shown with electrode components in Figure 9.

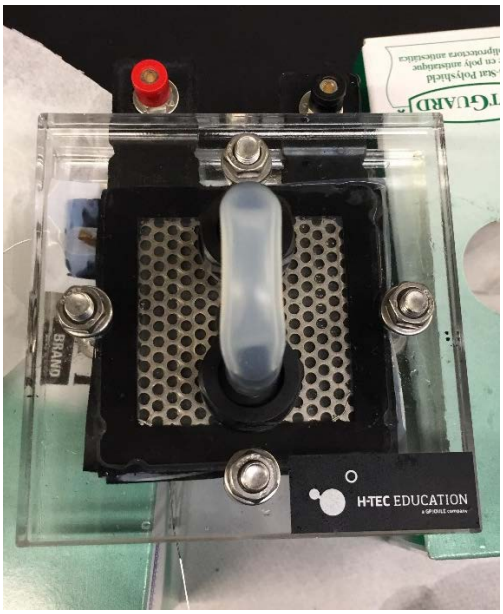

Figure 9: H-TEC PEMFC Kit

The kit allows for ease of disassembly, and consists of two current collectors, their respective carbon paper electrodes, and a Nafion™ membrane separator, all housed by rubber gaskets in close proximity. The Nafion™ membrane was replaced with our ionic redox transistor membrane for all tests. Unlike the Nafion™ membrane, the transistor membrane is an active ionic membrane, and cannot contact either of the carbon electrodes directly without short-circuiting the cell. For this reason, two additional Celgard separators (25 µm pores, 40% porosity) were added to the cell, one between each electrode and the transistor membrane. These additional separators were prepared by soaking in NaDBS, a surfactant, for at least 24 hours to increase their hydrophilic properties, then soaked in their respective half-cell solutions for several hours before the full cell was assembled. The full super-capacitor architecture is shown in Figure 10 below.

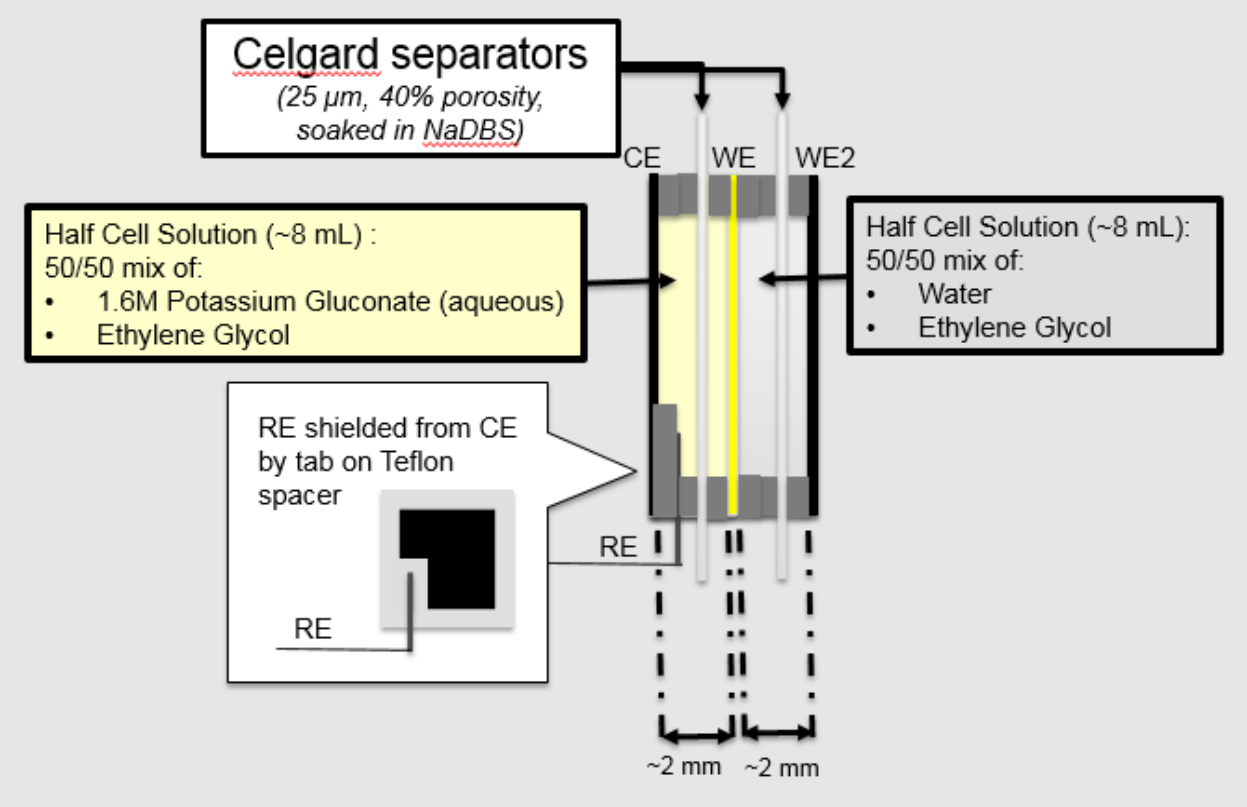

Figure 10: Super-Capacitor Architecture

The fuel cell kit was designed to operate using hydrogen and oxygen, or hydrogen and air. Since we modified the fuel cell to run on a semi-aqueous electrolyte and our set-up mimics the operation of a redox flow battery, the cell will be referred to as a flow cell going forward. The following images detail the flow cell assembly:

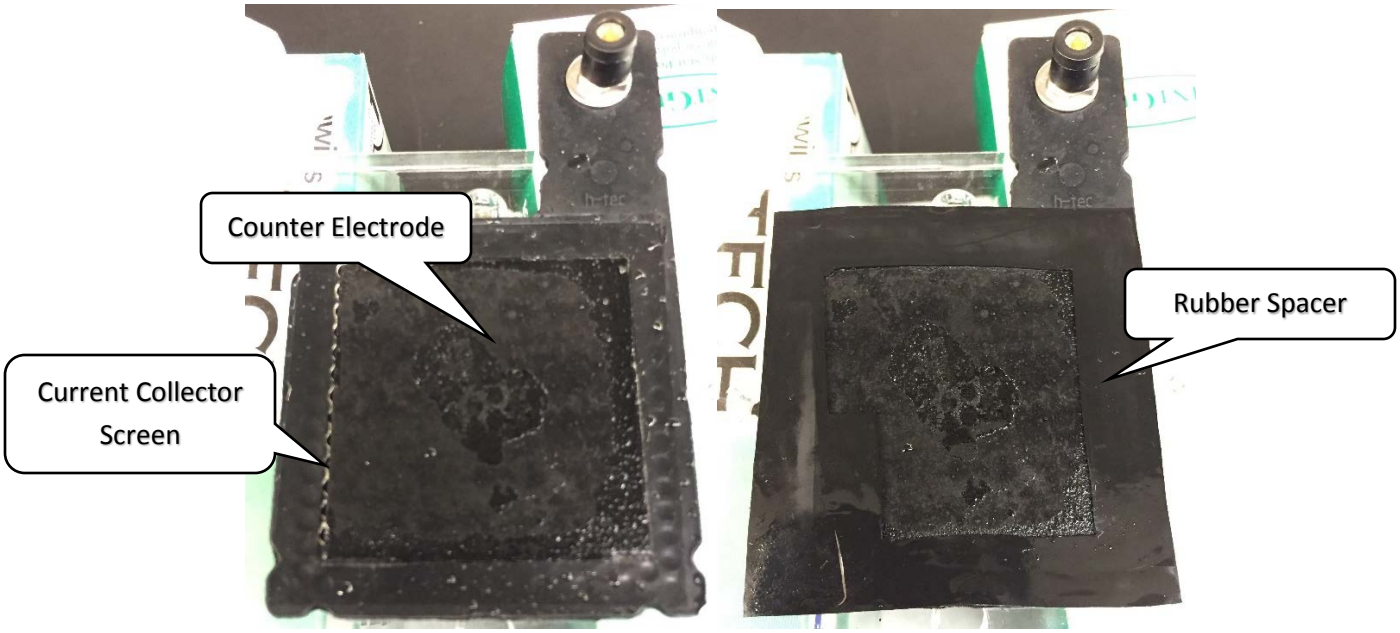

Figure 11: Wetted Carbon Electrode on Current Collector, Followed by Rubber Spacer with Tab

The first carbon paper electrode was wetted with DI water, and then placed in contact with its current collector. A rubber spacer was placed over the electrode/current collector with a protruding tab.

Figure 12: Reference Electrode Placement, Followed by Rubber Spacer

In Figure 12, a reference Ag/AgCl electrode made by setting a silver wire in chloride for 30 minutes was then placed on the rubber tab, electrically isolating it from the carbon counter electrode. This was then followed by another rubber spacer.

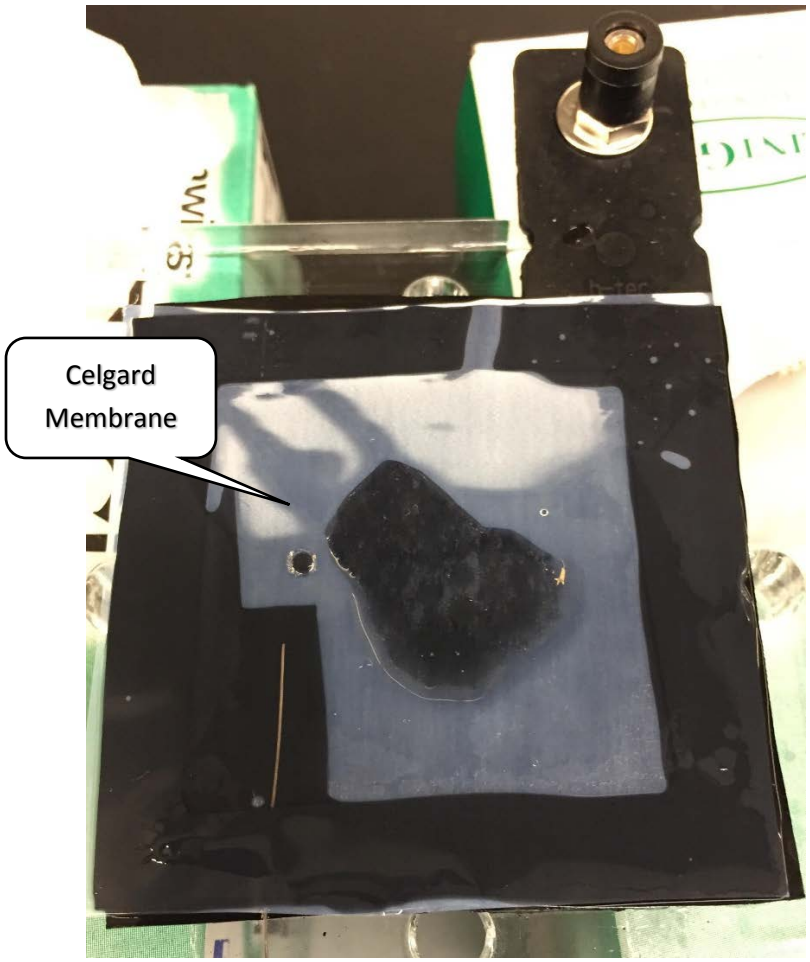

Figure 13: Addition of Celgard Membrane Separator

The first standard membrane separator was then laid over top of the rubber spacer. Several drops of potassium gluconate solution were added onto the separator to better wet it. Previous attempts to use membrane separators without soaking them in NaDBS or electrolyte solution resulted in poor ion transport characteristics. The dark area in the middle of the cell

from Figure 13 is a protruded portion of the carbon paper electrode in contact with the Celgard separator.

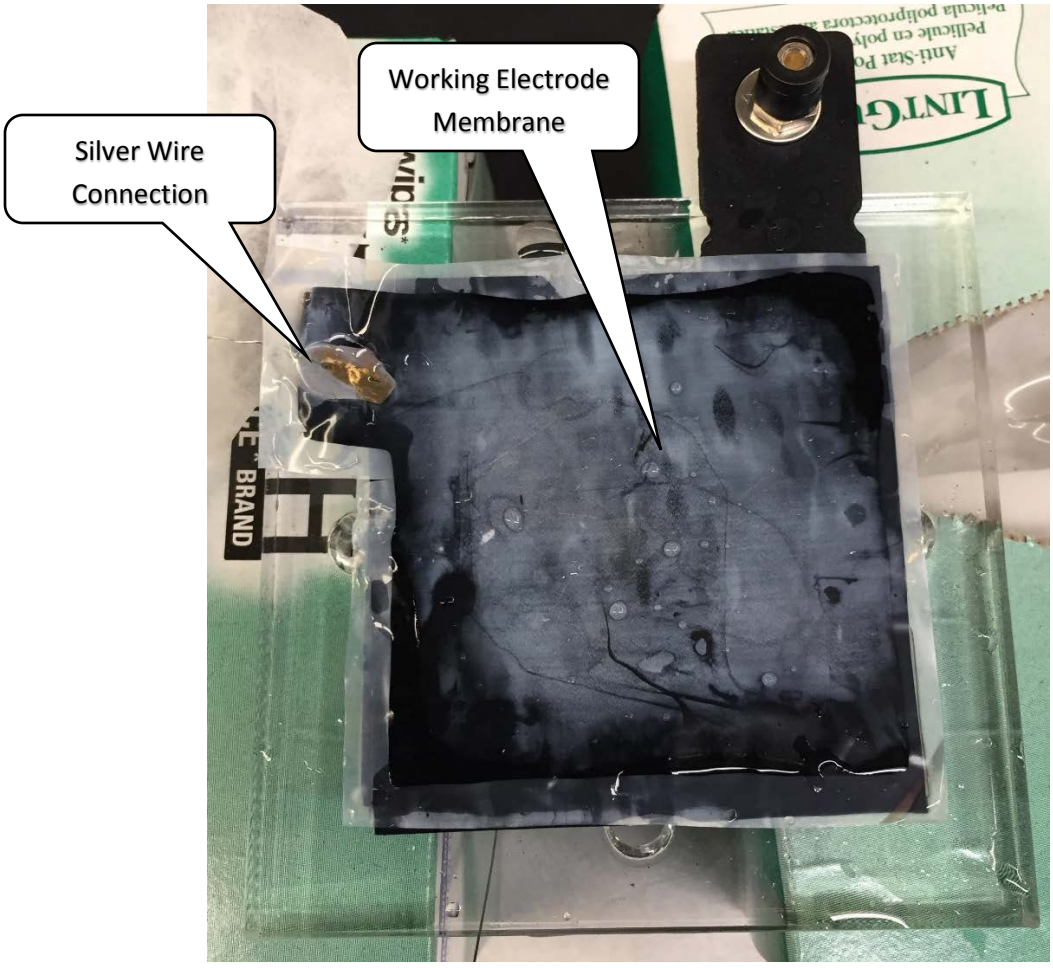

Figure 14: Addition of Transistor Membrane on Top of Celgard Separator

The transistor membrane was then placed face down over the Celgard separator, completely closing off the potassium gluconate half-cell. In this manner, the reference electrode can still accurately apply potential to the membrane. Though the transistor membrane has an area of 25 cm^2, the interfacial area of the flow cell restricts the effective usable area to 16 cm^2.

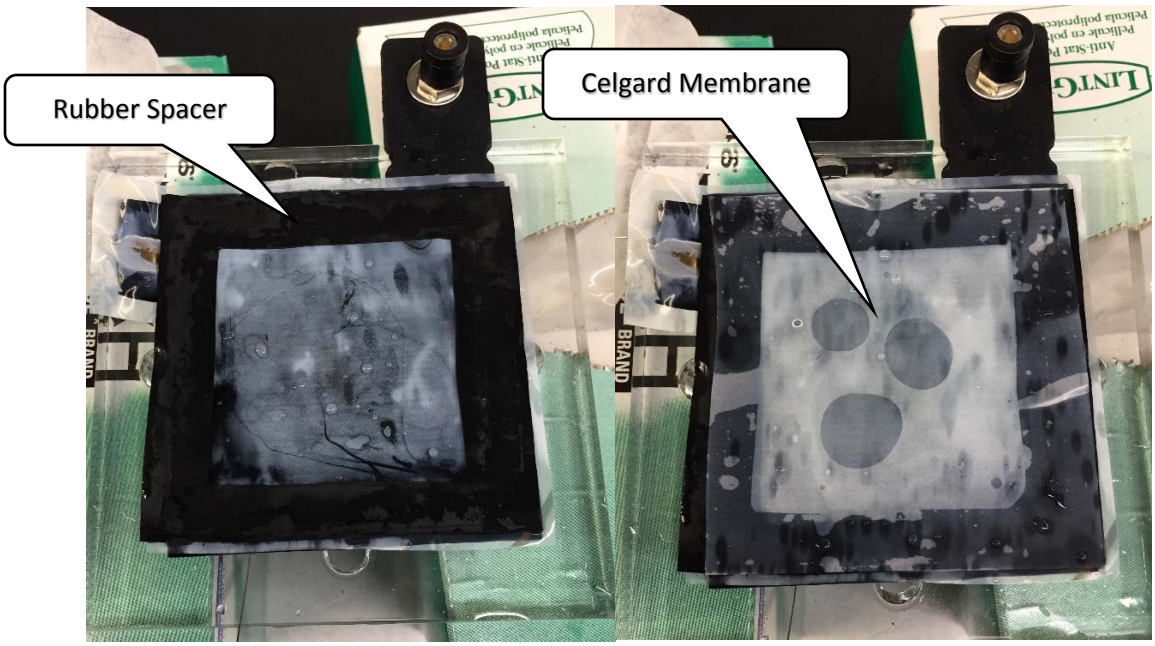

Figure 15: Addition of Rubber Spacer, then Celgard Membrane Separator

Once the transistor membrane was added, another rubber spacer was placed on top. Several drops of a 50/50 mix of DI water and ethylene glycol were placed on the back of the transistor membrane before adding the Celgard membrane separator, which had been soaking in an identical mixed solution. After the separator, another rubber spacer was added, shown below in Figure 16.

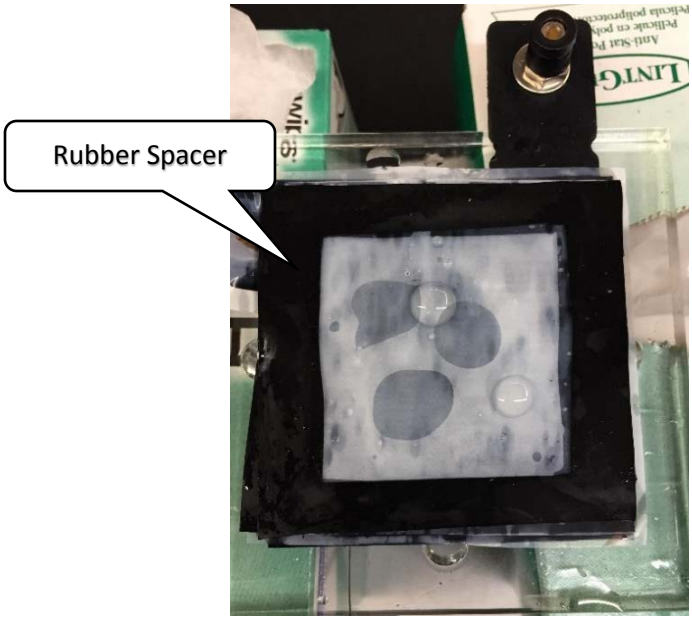

Figure 16: Addition of Rubber Spacer

After adding a few more drops of DI water and ethylene glycol, the second carbon paper electrode and its current collector were placed on top of the entire cell, and bolted into place (Figure 17). When fully tightened, the rubber gaskets and spacers create a water-tight seal with no leakage.

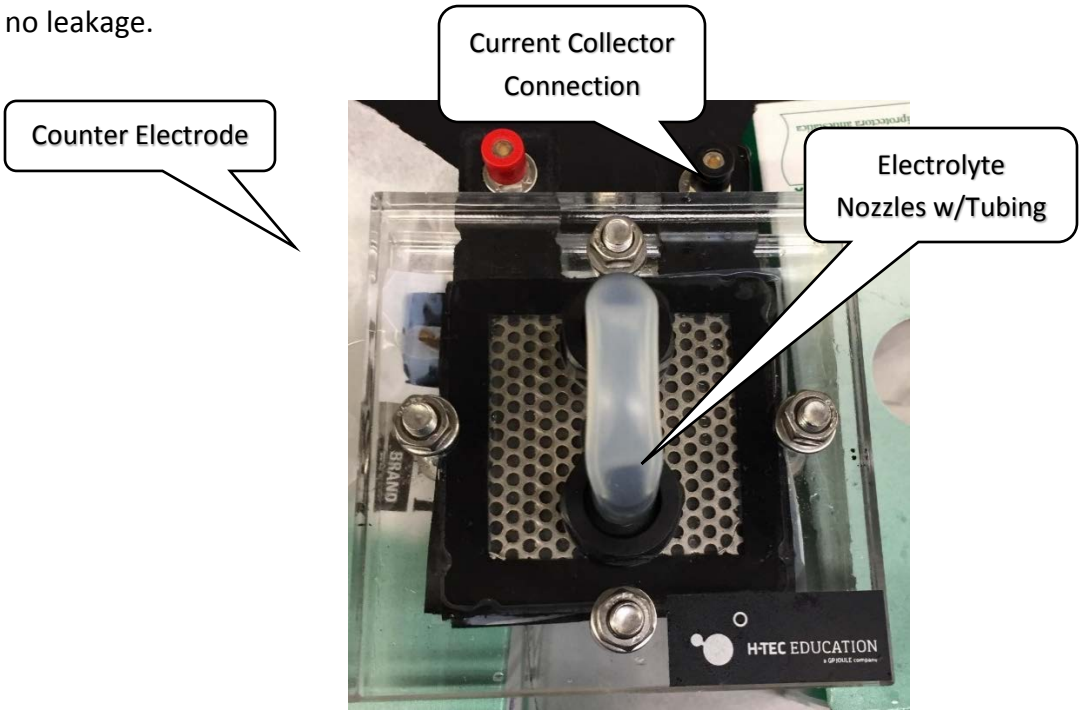

Figure 17: Addition of Carbon Electrode and Current Collect, Fully Assembled Cell

Each half-cell has nozzles connected by rubber hosing used to fill electrolyte. A true redox flow cell set-up would have external tanks that circulated electrolyte through each half-cell, but for the purposes of this research the nozzles were left connected together after electrolyte was introduced. Roughly 4 mL's of solution were added to each half cell chamber. Figure 18 displays the full super-capacitive flow cell electrically connected to the ElProScan ELP3 bipotentiostat.

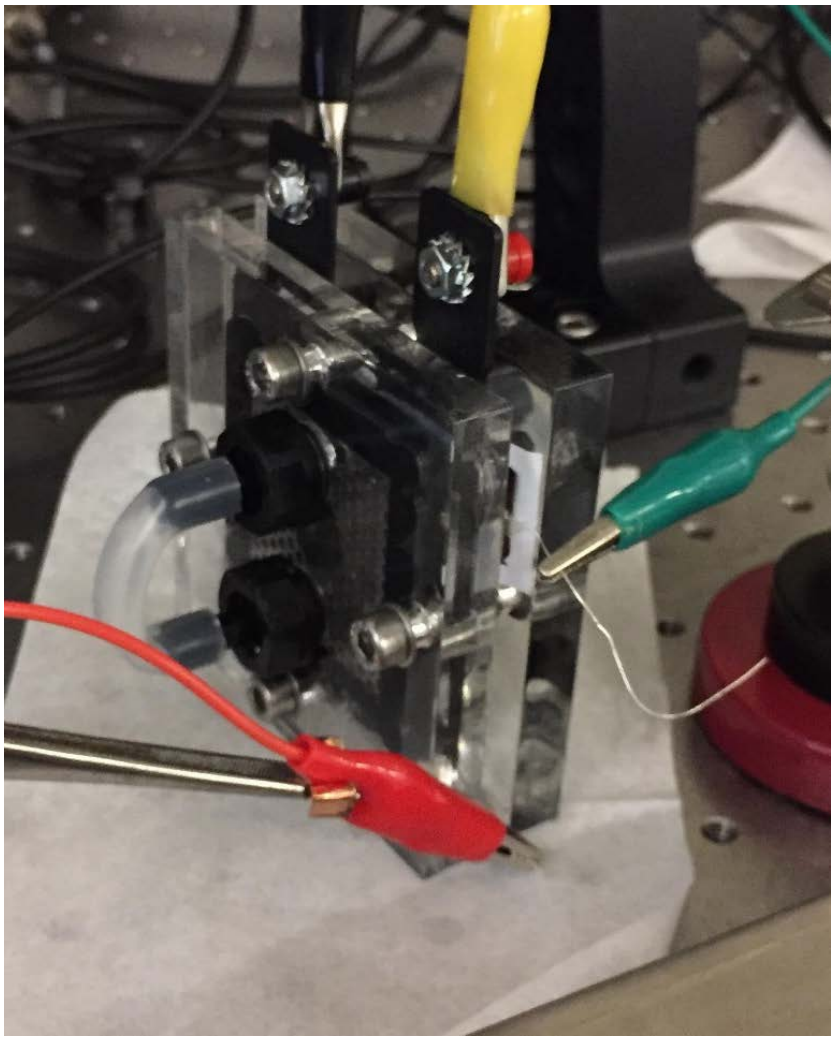

Figure 18: Fully Connected Flow Cell

2.3.4 Closed Cell Transmembrane Testing

Though the small Delrin™ membrane chamber and the large H-TEC flow cell use different architectures to construct a closed cell, the tests applied to them are identical. Transmembrane tests are the first series of tests designed to characterize the membrane's ability to mediate ion transport at a variety of potentials. All closed cell tests are performed using the ElProScan ELP3 bipotentiostat.

Before a transmembrane test begins, several CV cycles are recorded. These cycles confirm that the cell is electrically connected, and that the membrane is functioning as intended. The current response in these closed cell CV's is slightly different due to the new boundary conditions imposed on the membrane by the rubber spacers. These changes will be discussed further in Chapter 3.

After verifying the closed cell set-up is functional, a transmembrane test is conducted using the ElProScan ELP3 bipotentiostat. While an arbitrary voltage potential is applied to the membrane (shown as V_m in Figure 19), the transmembrane potential applied across the cell (V_{ac}) is alternated from positive to negative several times, allowing measurement of both charge and discharge throughput current (I_{ac}) across the membrane.

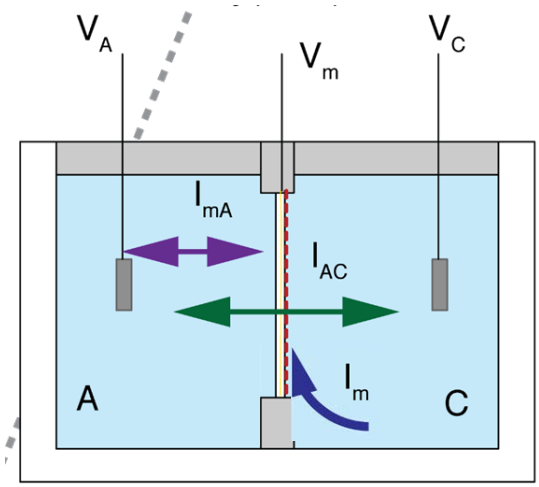

Figure 19: Closed Cell Schematic (Hery, 2016)

This process is repeated over an array of membrane potentials (V_m) determined by the particular membrane CV. The array generally starts at 0 V, then sweeps down to the reduction peak potential in 0.1 V increments. Once the reduction potential is reached, an upsweep of the same potential increments is applied until the oxidation peak potential is reached. Each potential interval lasts between 80-120 seconds depending on how long it takes the current response to reach steady state. V_{ac} can be any number of alternating signals, but is usually a square wave or sine wave alternating between -1 and 1 V. Throughout the duration of the transmembrane test, I_{ac} and I_m are recorded.

Note that the transmembrane current data collected in these tests does not contain true I_{ac} and I_m, but rather a combination of these currents and the interplay current I_{ma}. . I_{ma} in the above figure is a current resulting from the differences in potentials applied from the reference electrode to the working membrane electrode and working counter electrode. A correction will be applied to the data after collection to remove this interplay current from the results. Both small and large membrane cells experience this interplay current. There are no

notable differences between transmembrane tests for small and large membranes other than slightly different values for reduction and oxidation peak potentials.

2.3.5 Forced Charge Testing

Whereas transmembrane testing is characterizing membrane ion transport at several potentials during an alternating transmembrane potential, forced charge tests are conducted at two potential values indicative of the membrane's redox states while applying a constant negative transmembrane potential. This configuration allows characterization of steady state membrane ion transport while the membrane is in its binary ON and OFF states and the super-capacitor is being charged.

CV cycles are conducted before testing to verify electrical connectivity and a working membrane. After cycling, the transmembrane potential (V_{ac}) is set to -1 V while the membrane potential (V_m) is set as the reduction peak potential. This configuration is held for up to an hour, long after the transmembrane current has reached steady state. The membrane potential is then set to the oxidation peak potential, and the transmembrane current response is recorded over the same duration of time. This oxidized configuration is a fair estimation of the worst case scenario for self-discharge of the cell.

To better characterize the membrane's contribution to steady state current in these tests, a baseline experiment was also conducted, which used three layers of plain Celgard as the only separator material between the anode and cathode portions of the flow cell. Steady state current from this test can be compared to steady state tests with the membrane to identify how the conducting polymer component of the membrane affects self-discharge.

2.4 Data Analysis

2.4.1 MATLAB Post-Processing and Correction

Data from the ElProScan ELP3 bipotentiostat was exported as several arrays. These arrays were imported to MATLAB for plotting and analysis. While open cell data was directly plotted with no alterations, the transmembrane closed cell test data required correction to remove the influence of the interplay current (I_{ma}) on transmembrane current (I_{ac}). Closed cell forced charging tests also have this interplay current I_{ma} included in both plots for I_{ac} and I_m, but since current readings for I_m go to zero over time, and only steady state reading in these tests are important, it can be concluded that steady state I_{ac} is not affected by I_{ma}, and therefore needs no correction. Transmembrane tests involve quickly changing intervals, which does not allot enough time for currents to reach steady state, necessitating correction.

Both transmembrane currents (I_{ac} and I_m) contain the interplay current. I_m is the current associated with the redox states of the membrane, and is transient during the time immediately after changes in the membrane's redox potential. However, once this transience ends and there are no more redox events taking place, the current associated with redox potential goes to zero, and the remaining current (I_{ma}) can be attributed solely to the interplay effects from potential differences between the two working electrodes. This interplay causes formation of a double layer of ions at both membrane and working carbon electrode surfaces. The charge of the membrane double layer is equal and opposite to that of the charge of the working carbon electrode. Therefore, to remove interplay effects from the transmembrane current (I_{ac}) measured at the working carbon electrode, the steady state current I_m^{ss} is added to

I_{ac} to produce a corrected current array I_{ac}^{C}. In practice, the entire I_m array is added to the entire I_{ac} array, as the transient states are not used or considered for analysis.

2.4.2 Transistor Curves

To better summarize the membrane's ion transport properties at each potential increment, a MATLAB code was used to find the maximum and minimum current values at the last transmembrane potential cycle of each redox potential (V_m) value. These maximum and minimum values correspond to the steady state peak-to-peak current values found each redox potential. The current values, when plotted against the redox potential values, provide a transistor curve denoting the peak-to-peak current performance of the membrane across all possible membrane potentials. From this curve, an amplification factor can be found which identifies the factor of increase in current between the membrane's oxidized OFF state and its fully reduced ON state. The factor is obtained by dividing the peak-to-peak fully reduced current by the peak-to-peak fully oxidized current. These curves and factors are useful in identifying cell performance and characterizing membrane transport properties.

2.5 Conclusion

In Chapter 2, we explored the methodology behind setting up and running the experiments that comprise this research paper. Techniques used to fabricate and characterize membranes, set up membranes within cells, and run several types of electrochemical tests have been discussed, as well as the ways in which the resultant data is corrected and plotted for the purpose of useful analysis. Much of the same terminology and denotation of particular currents

and potentials will carry into Chapter 3, where the results from the tests mentioned in this chapter will be displayed for the purposes of analysis and discussion.

Chapter 3: Results, Analysis and Discussion

3.1 Introduction

In this section, data collected using the methods previously discussed will be presented and discussed. This compilation consists of cyclic voltammetry cycles that characterize individual membranes, charge storage data derived from those CV cycles, and multiple types of closed cell tests. All tests are conducted in a potentiostatic configuration, with set potentials or potential rates and observed current and charge data. Within this chapter, the description 'open cell' refers to the three-electrode setup in which the working electrode membrane is placed in an ionic solution. The 'closed cell' term refers to the membrane placed between two half-cells in a four-electrode configuration. All CV's are shown with current on the y-axis and potential on the x-axis, and individual axes have unit parameters included. Current density for all membrane samples in this thesis is consistently 1.5 C/cm^2

3.2 Small and Large Scale Membrane Open Cell CV Comparisons

As mentioned in section 2.3.1, after a 0.3 cm^2 membrane was polymerized and equilibrated for 20-30 cycles in an open cell, its CV would exhibit relatively consistent current response from cycle to cycle. Figure 20 displays an example of such a CV, which represents the majority of small-scale membranes well. The first cycle of each CV deviates slightly from the steady-state reponse, and should not be used to determine current or potential values.

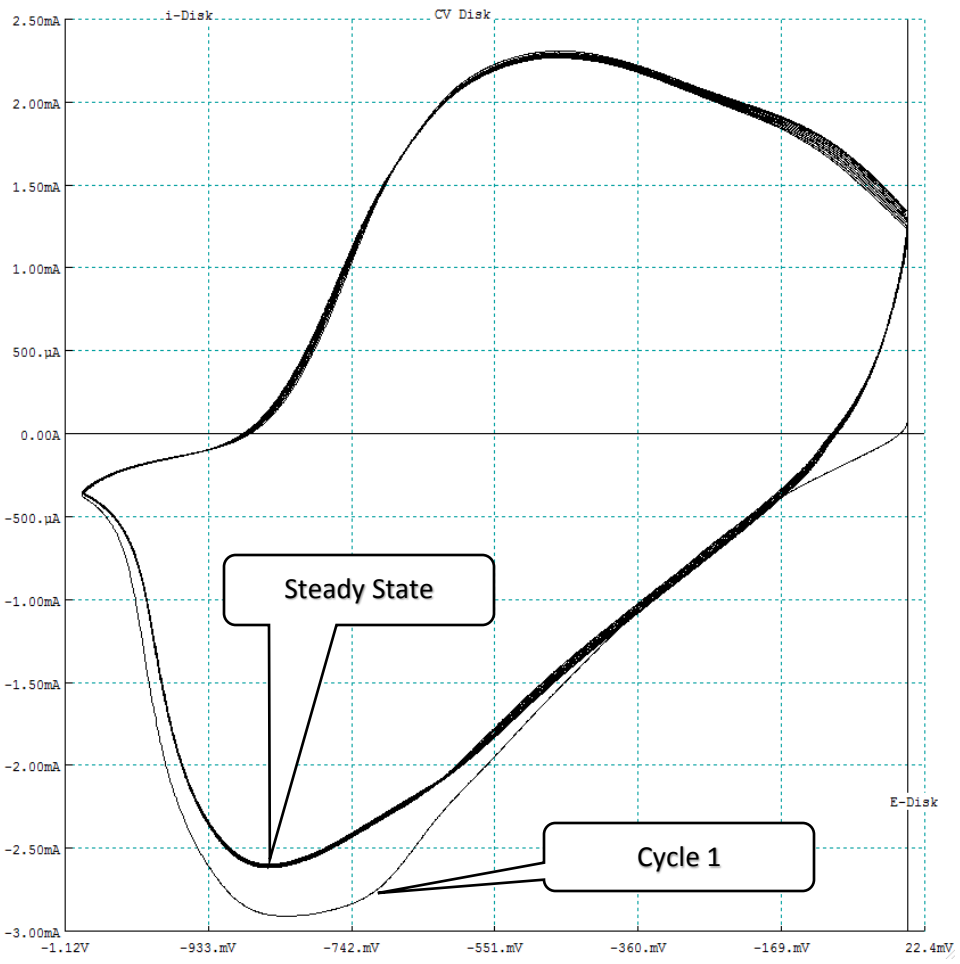

Figure 20: Small Scale Membrane Open Cell CV

Based on the thicker, converged lines, this particular membrane has a reduction peak current of around 2.6 mA, occurring around -850 mV, and an oxidation peak current of 2.3 mA occurring around -450 mV. Peaks of this magnitude are a fair representation of most small samples of membrane tested. Note that these peak currents do not represent the steady state current of the membrane that would result from a constant applied potential, but are more a measurement of the instantaneous rates of ion ingress at each potential level. The limit to the rate of ion movement into and out of the polymer is determined by how quickly ions can move into the immediate surroundings of the membrane via diffusion. The maximum rates at the

peaks represent these limits, as any potential outside either peak exhibits decreased rates of ion movement.

Before cycling the first larger membrane that was created, it was theorized that such a membrane would exhibit larger peak reduction and oxidation currents when compared to the smaller scale membranes. Estimates stated that since the large membrane surface area increased by about a factor of 83, the resultant peak currents would increase by about the same factor, and would be found around the range of 200 mA. The inherent assumption of this estimate is that membranes of identical charge density will exhibit identical throughput current per unit area. Through experiment, the larger membrane CV's, as exemplified in Figure 21, had peak currents that did not reach the values predicted by the initial estimate.

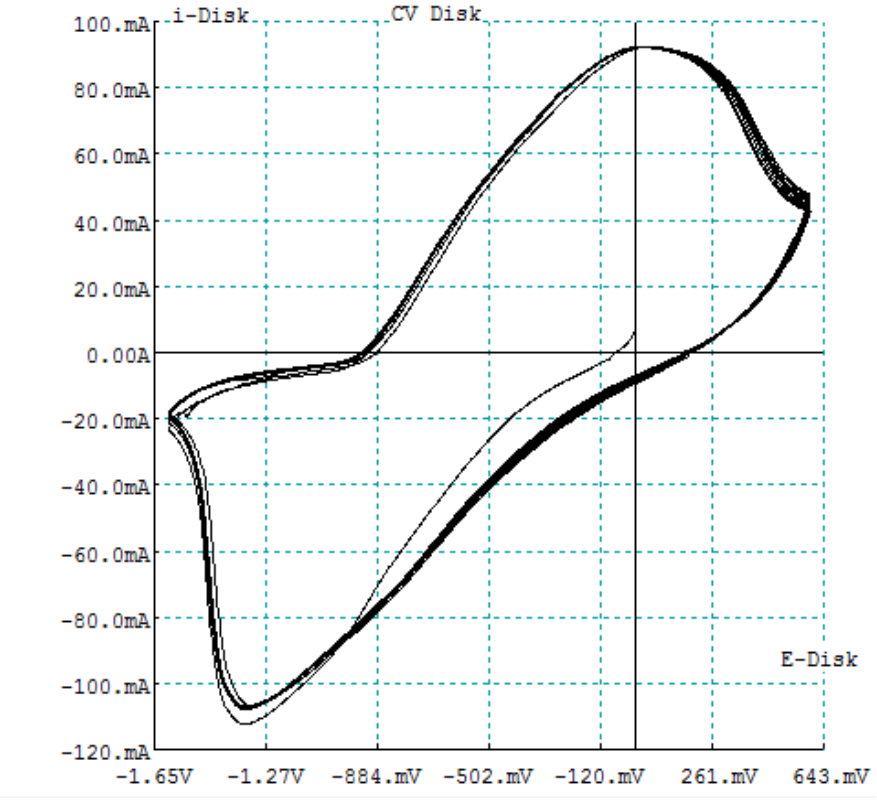

Figure 21: Large Membrane Open Cell CV

One reason for the disparity between the theoretical and experimental results may be increased resistance in the larger membrane electrode. Current must travel through a longer mean path through the larger electrodes, resulting in ohmic losses. It is also important to take into account the geometric constraints of both chambers when comparing CV's. The smaller membrane is immersed in a comparatively large beaker of electrolyte, which allows for electrolyte to diffuse more readily towards the surface of the membrane. The polymerization chamber for the larger membrane, however, has limited space for diffusion due to the walls of the chamber closely matching the perimeter of the membrane. This constrained space can therefore directly affect the reduction and oxidation peaks, as they represent the maximum rate at which ions can diffuse into the immediate area of the membrane via Brownian motion. Both ohmic losses and diffusion-related geometric constraints are reasonable explanations for the differences between the extrapolated small membrane CV estimate and the actual larger membrane CV.

Another important item of interest that comes from a CV is the amount of charge that moves into and out of the membrane during its respective reduced and oxidized intervals. This information can be derived through integration of the current data collected, but is also automatically plotted by the ElProScan ELP3 bipotentiostat. Figure 22 displays the charge storage of a small scale membrane during several CV cycles, which can be directly compared to Figure 23 which displays the same data collected from a large scale membrane. The y-axis depicts charge in millicoulombs (mC).

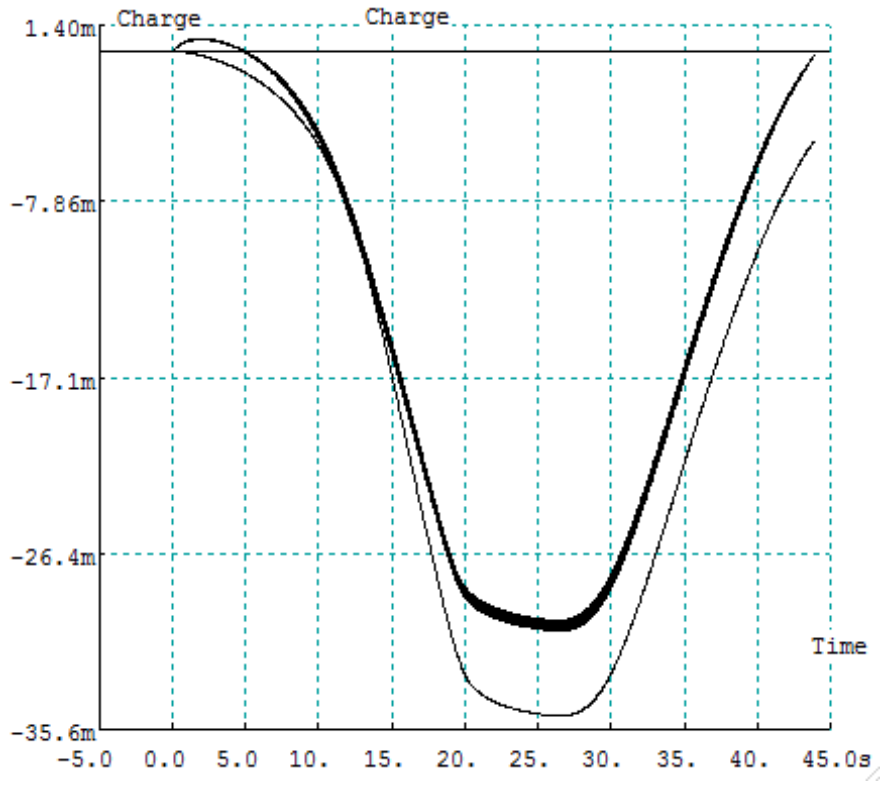

Figure 22: Charge Storage of Small Membrane in Open Cell

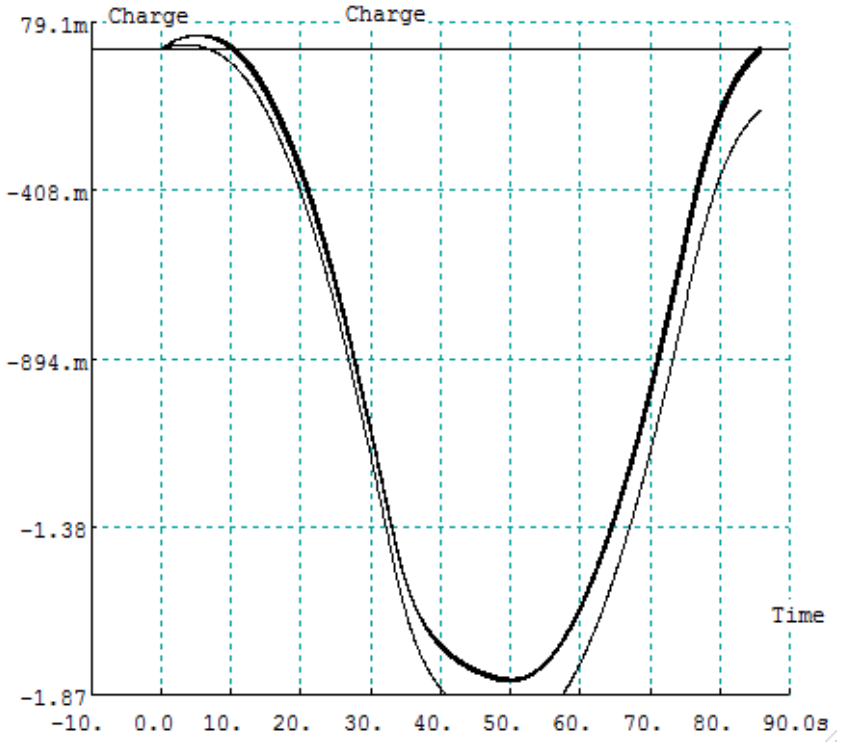

Figure 23: Charge Storage of Large Membrane in Open Cell

Each convex sweep represents a CV cycle, with charge accumulation occurring during the reduced interval and charge dispersion occurring during the oxidized interval. Once reaching steady state, the small membrane is capable of storing roughly 30 mC, while the larger membrane can store around 1.8 C of charge. This roughly 60-fold increase in charge storage is a definite improvement for this first generation of large membranes, though it falls short of the estimated storage increases for the same reasons discussed above.

3.3 Small and Large Scale Membrane Closed Cell CV Comparisons

Besides the persistence of limited diffusion in closed cell chambers, the CV's from these configurations are altered due to the boundary conditions imposed on the membrane edges. The closed cell CV for the small membrane shown in Figure 24 depicts this difference.

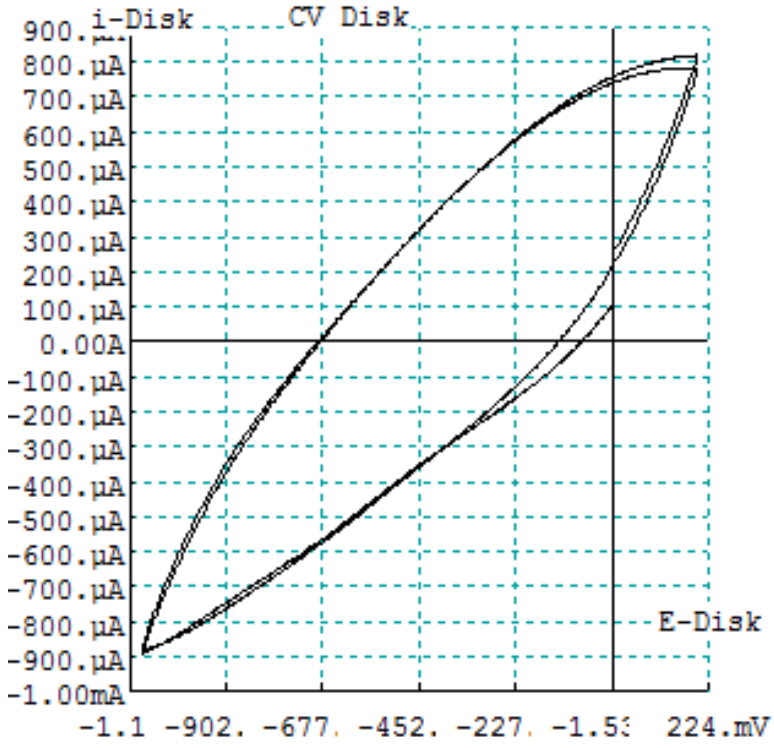

Figure 24: Small Membrane Closed Cell CV

The reduction and oxidation peaks are not reached over this voltage range, which is common in this particular closed cell set-up where the carbon counter electrode is farther away from the membrane. In addition, the reduction and oxidation currents have decreased significantly. This decrease also occurs in the flow cell CV, shown in Figure 25.

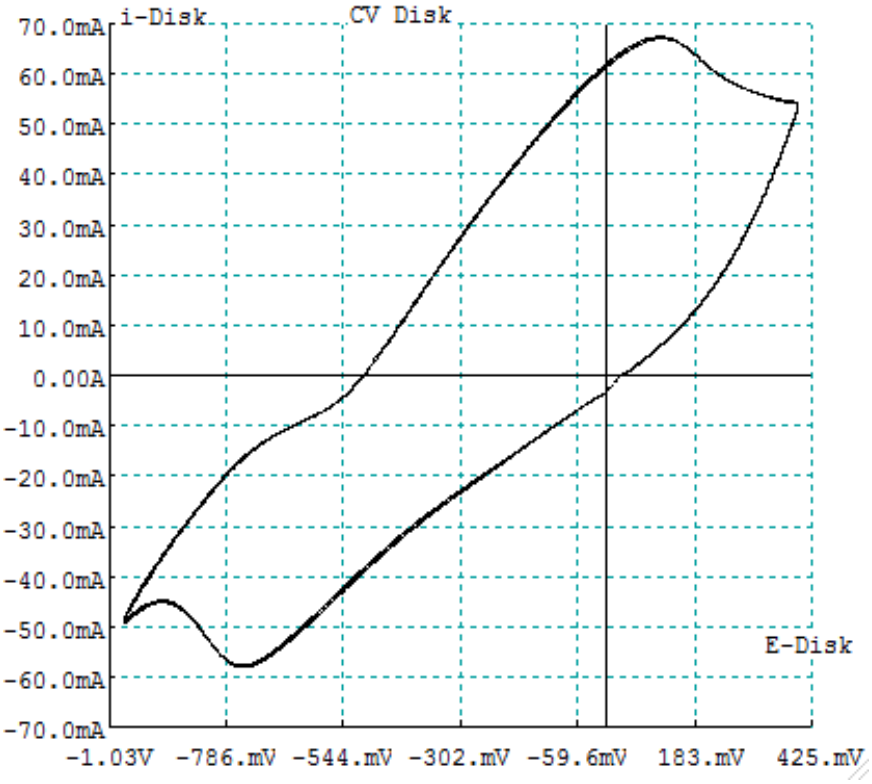

Figure 25: Large Flow Cell CV

Within the flow cell, the additional Celgard separators further limit diffusion and add to the overall resistance of the cell. Though a reduction in current amplitudes is an inherent issue with added separators, the close proximity of active electrical elements necessitates their inclusion. Such a configuration allows for closer reduction and oxidation peaks, which indicates a decrease in the irreversibility of the cell processes.

Charge storage is similarly impacted in closed cells. Figure 26 and 27 illustrate the reduction in charge storage of the respective small and large closed cells with respect to their open cell counterparts.

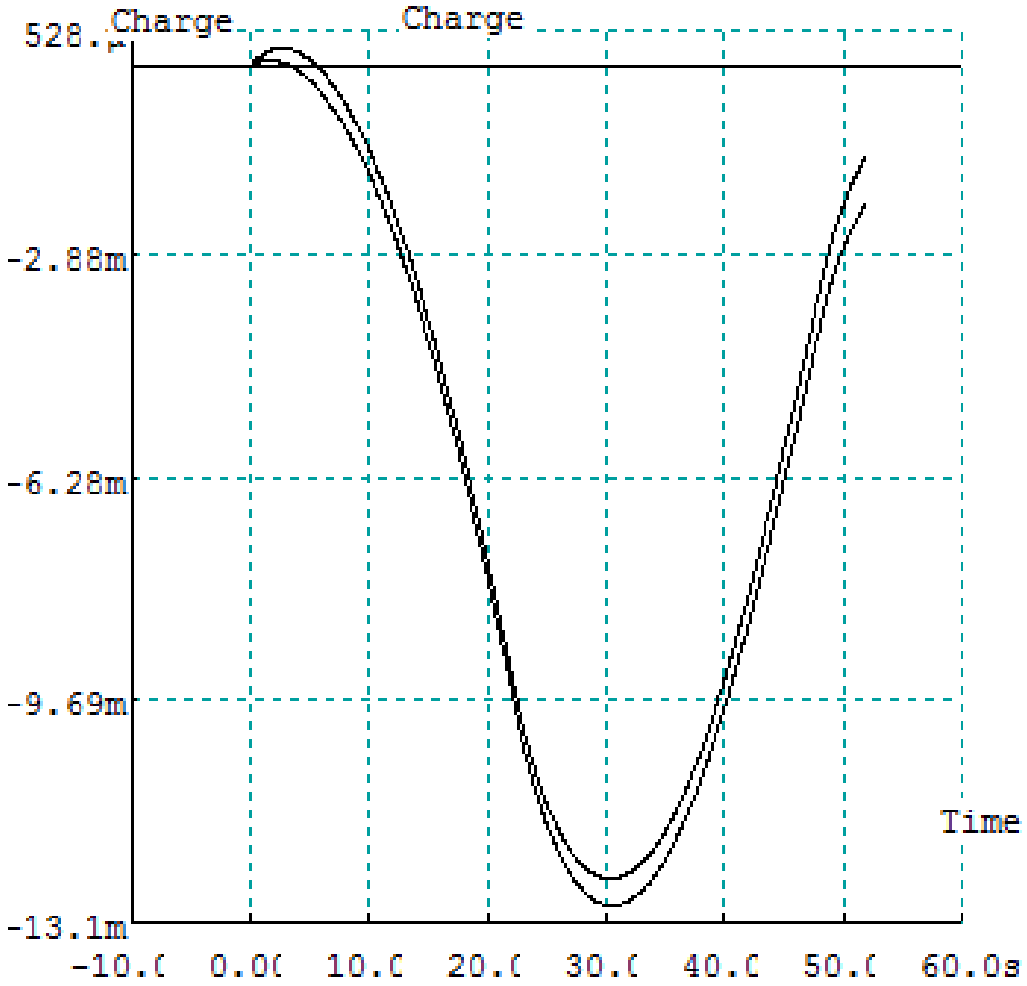

Figure 26: Charge Storage in Small Membrane Closed Cell

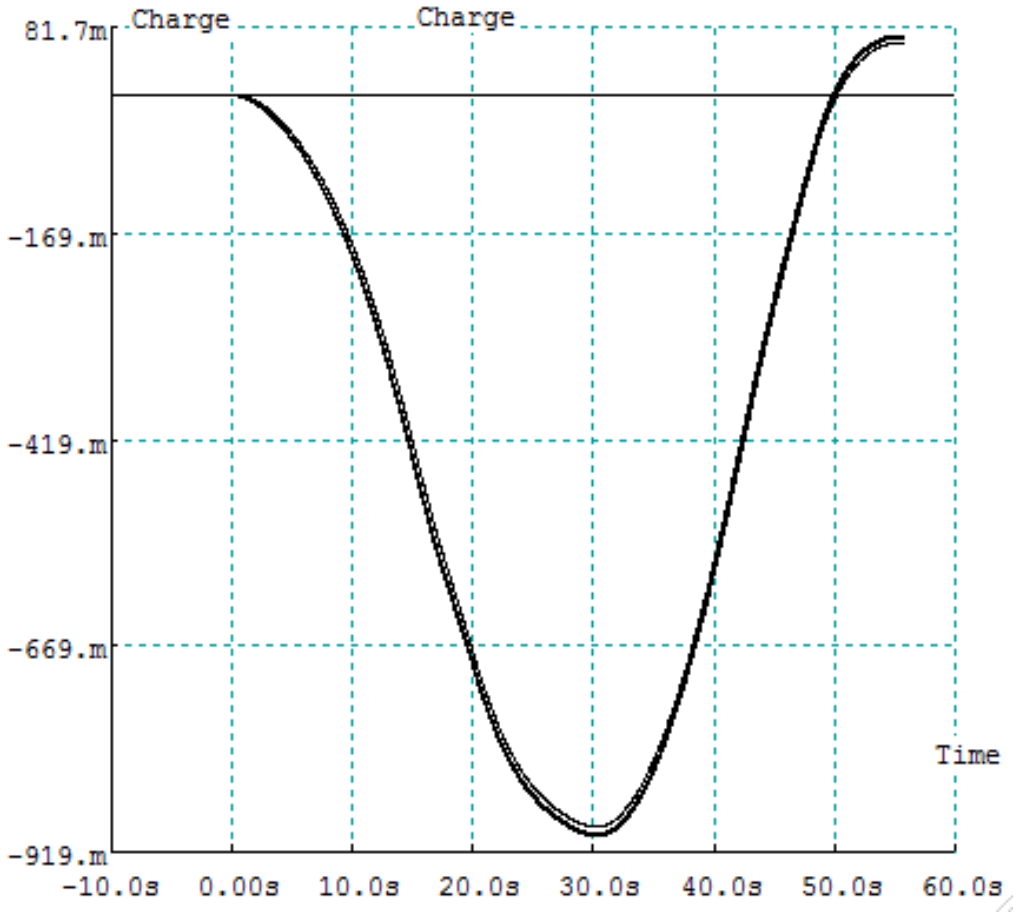

Figure 27: Charge Storage in Flow Cell

Getting the flow cell to produce these results took several iterations of separator preparation. Initial designs placed Celgard separators directly into the flow cell with no preparation, which resulted in little to no ion transport due to the hydrophobic characteristics of these particular separators. Attempts to soak the separators in NaDBS only before assembling the cell were occasionally successful, with some tests failing to track potential correctly and others failing to transport a significant amount of ions. Soaking the separators in NaDBS for 24 hours, then soaking in their respective half-cell solutions a few hours before assembly yielded the most consistent results.

3.4 Transmembrane Testing Comparisons

Knowing the characteristics of the closed cells from the previous section, a transmembrane test can be conducted using the potential ranges identified in the closed cell CV's. Figure 28 displays a full small cell transmembrane sweep starting at 0 V, descending to -1.1 V in intervals alternating between 0 V and the next reduction value. Once reaching the reduction peak potential, an upward sweep is conducted, alternating between the most negative reduction potential and each gradually increasing potential value. The test concludes when the oxidation peak potential is reached. V_{ac} was set as a 2 Hz sine wave for these tests as a high frequency wave would output currents associated with the capacitance of the cell while avoiding the resistances in parallel with those capacitive elements. The middle plot in the figure is membrane current, while the bottom-most plot is transmembrane current. The plots shown have had the MATLAB correction discussed in section 2.4.1 applied.

The particular test displayed was conducted with a solution of 1.6 M potassium gluconate with no ethylene glycol added. Previous tests with various ionic concentrations have shown a roughly proportional relationship between concentration and current, meaning that running the same test with a solution of 0.8 M potassium gluconate in a 50/50 mix of water and ethylene glycol could be estimated to produce half the current amplitudes this test displays.

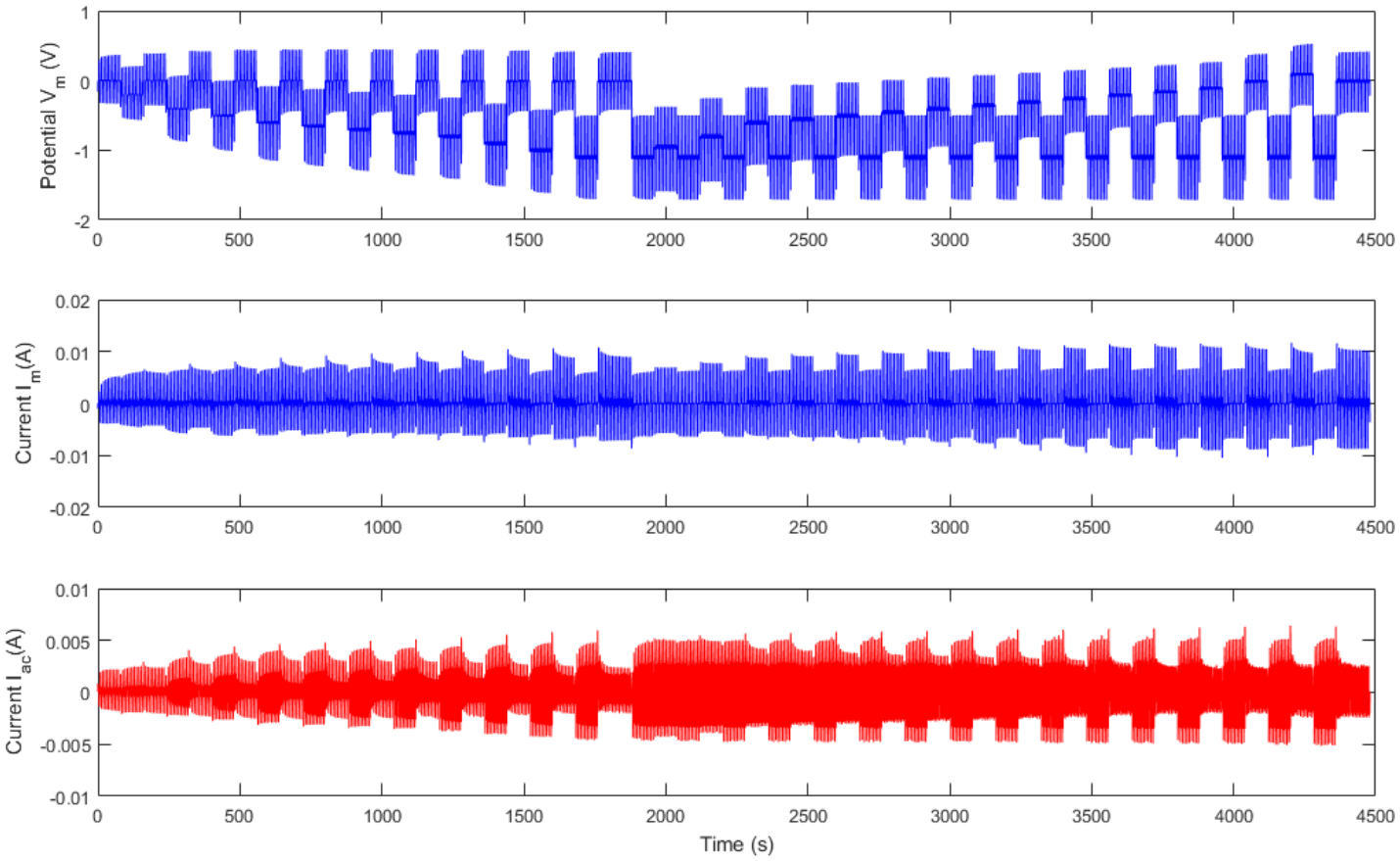

Figure 28: Small Cell Transmembrane Test

From the bottom subplot, it can be observed that the peak-to-peak current values are larger at more negative potentials, and and smaller at potentials near 0 V. The transmembrane plot itself imparts a good understanding of the test structure and general current amplitudes at each potential, but the transistor curves pulled from this plot provide a better summary for analysis. Figures 29 and 30 display the down-sweep and up-sweep curves from this test.

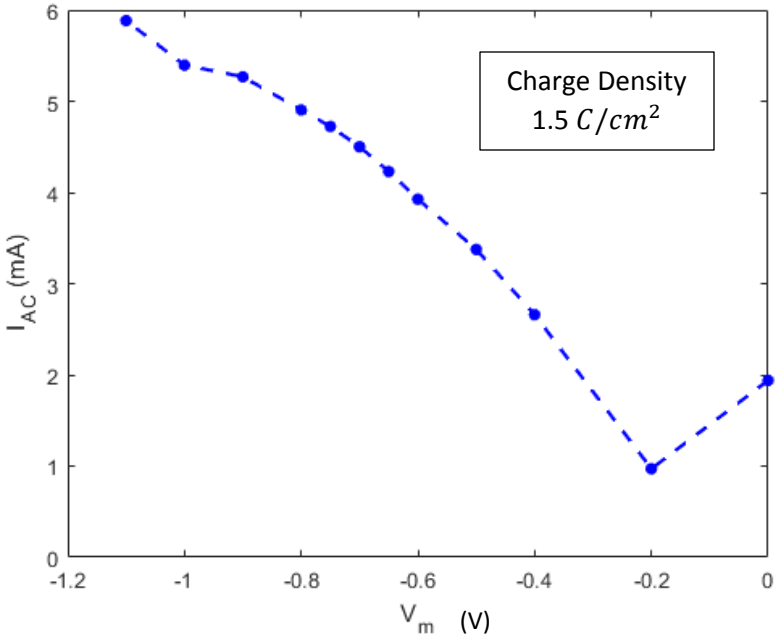

Figure 29: Down-sweep Transistor Curve

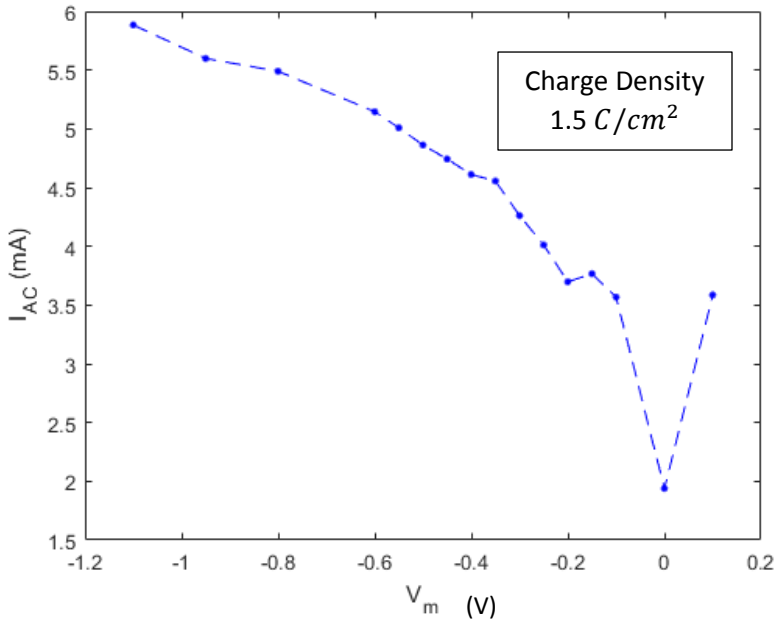

Figure 30: Up-sweep Transistor Curve

Some hysteresis is present, especially near the more positive potentials, but these curves give a reasonable estimate of the amplification factor between the oxidized and reduced

states. Averaging amplification factors between the sweeps (3 for upsweep, 6 for down-sweep) returns a factor around 4.5. There's a large margin of error for this factor, as small changes in the lowest oxidized current can change the value dramatically, but its reasonable in terms of estimating performance of the membrane.

Figure 31 displays the transmembrane test for the flow cell, of which V_{ac} was set as a square wave which alternated between -1 and 1 V in 4 second intervals.

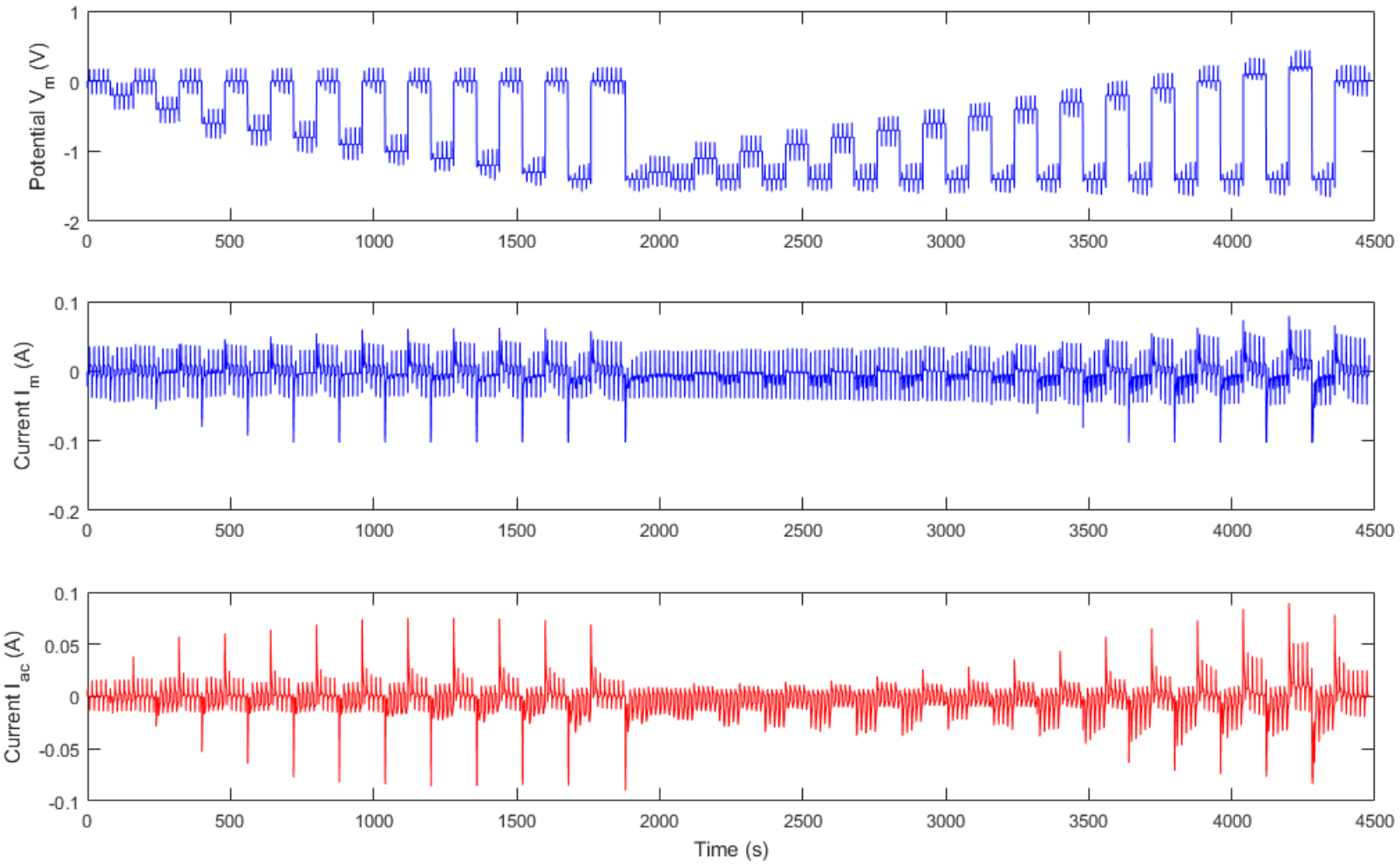

Figure 31: Flow Cell Transmembrane Test

This test was performed in a solution of 0.8 M potassium gluconate in a 50/50 mix of water and ethylene glycol. From this data, the peak-to-peak current values are pulled from the end of each potential interval, and plotted in down-sweep and up-sweep transistor curves, shown in Figures 32 and 33.

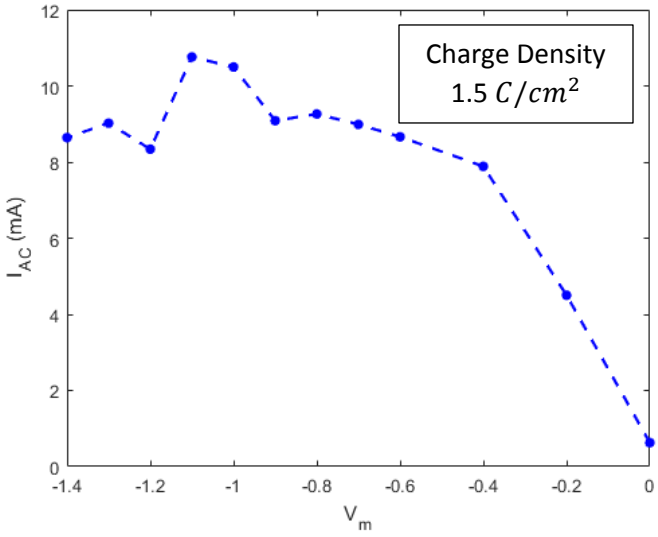

Figure 32: Down-sweep Transistor Curve

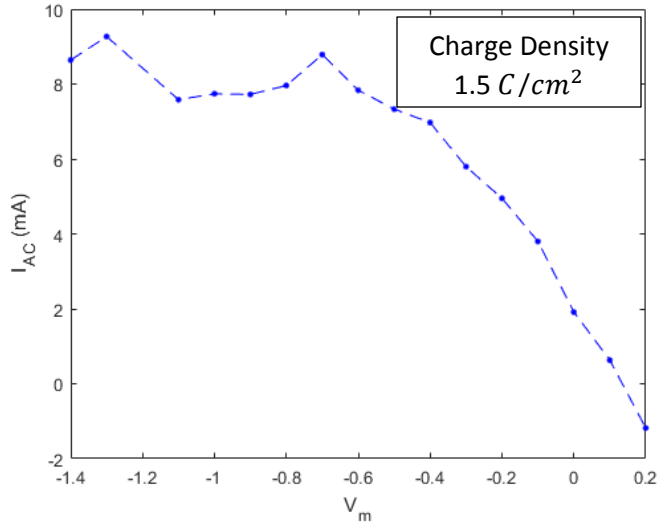

Figure 33: Up-sweep Transistor Curve

Like the small closed cell curves, there is some hysteresis between the sweeps. Calculating amplification factors using the reduction current at 1.3 V and the oxidation current around 0 V to 0.1 V, we obtain an average amplification factor of 14.5. As with the small closed cell transistor curves, this factor likely has a healthy margin of error, and is primarily useful for obtaining a ballpark estimate of cell performance, though it can be concluded that the large membrane allows much larger throughput currents when compared to its smaller scale counterpart.

3.5 Forced Charge Test Comparison

Forced charge tests are relevant to scenarios involving self-discharge, and demonstrate in a clear manner the ionic redox transistor membrane's ability to control ion transport when charging and discharging the cell. Figure 34 displays a small membrane forced charge test where the cell is constantly charging at -1 V during membrane redox potentials at both -1.1 V and 0.1 V. There exists some transience during the period immediately after the membrane potential is switched from -1.1 V to 0.1 V. Due to the nature this test, the only areas of importance are when I_m goes to zero (and the interplay current I_{ma} discussed in section 2.4.1 can be neglected). For this reason, sections of the transient data are outside the range of the figure in order to provide a better view of the steady-state regions.

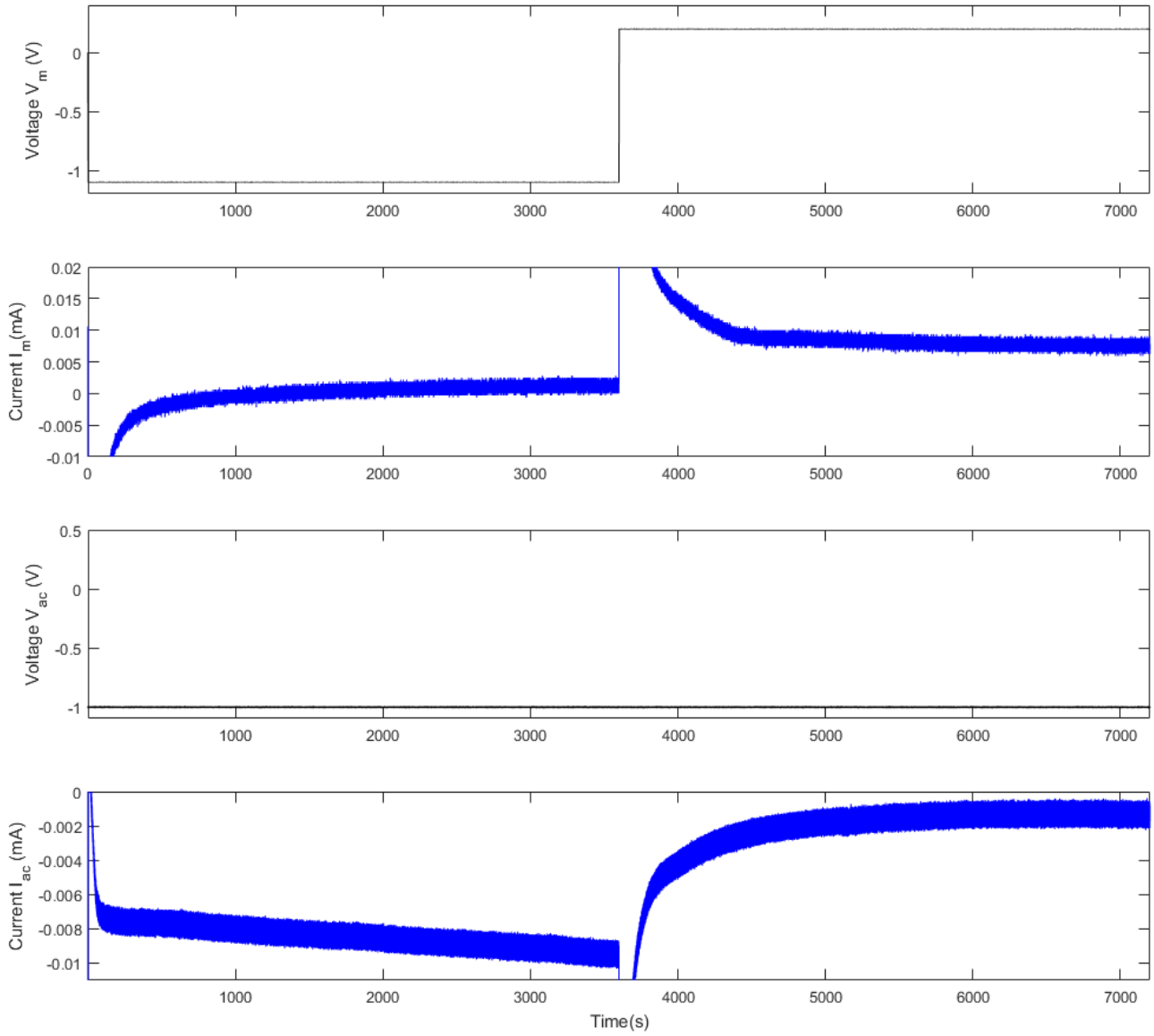

Figure 34: Small Membrane Forced Charge Test

Note that though this test is conducted over large timescales, the reduced transmembrane current fails to reach steady state before the oxidized interval begins. This transience implies holding the cell potential at -1 V requires increasing rates of charge movement, which translates to slowly increasing leakage currents. Over the oxidized interval, the transmembrane current reaches a steady state at very low levels, signifying the oxidized PPy(DBS) membrane significantly limits leakage current and allows the cell to better hold

charge without need for additional input. It should also be noted that the membrane current I_m reaches steady state at a non-zero value after redox events have settled down, implying some amount of interplay current I_{ma} is still influencing the super-capacitor. The same forced charge test was applied to the flow cell (Figure 35). Based on the CV from Figure 25, the reduction potential was set as -750 mV and the oxidation potential was set as 150 mV.

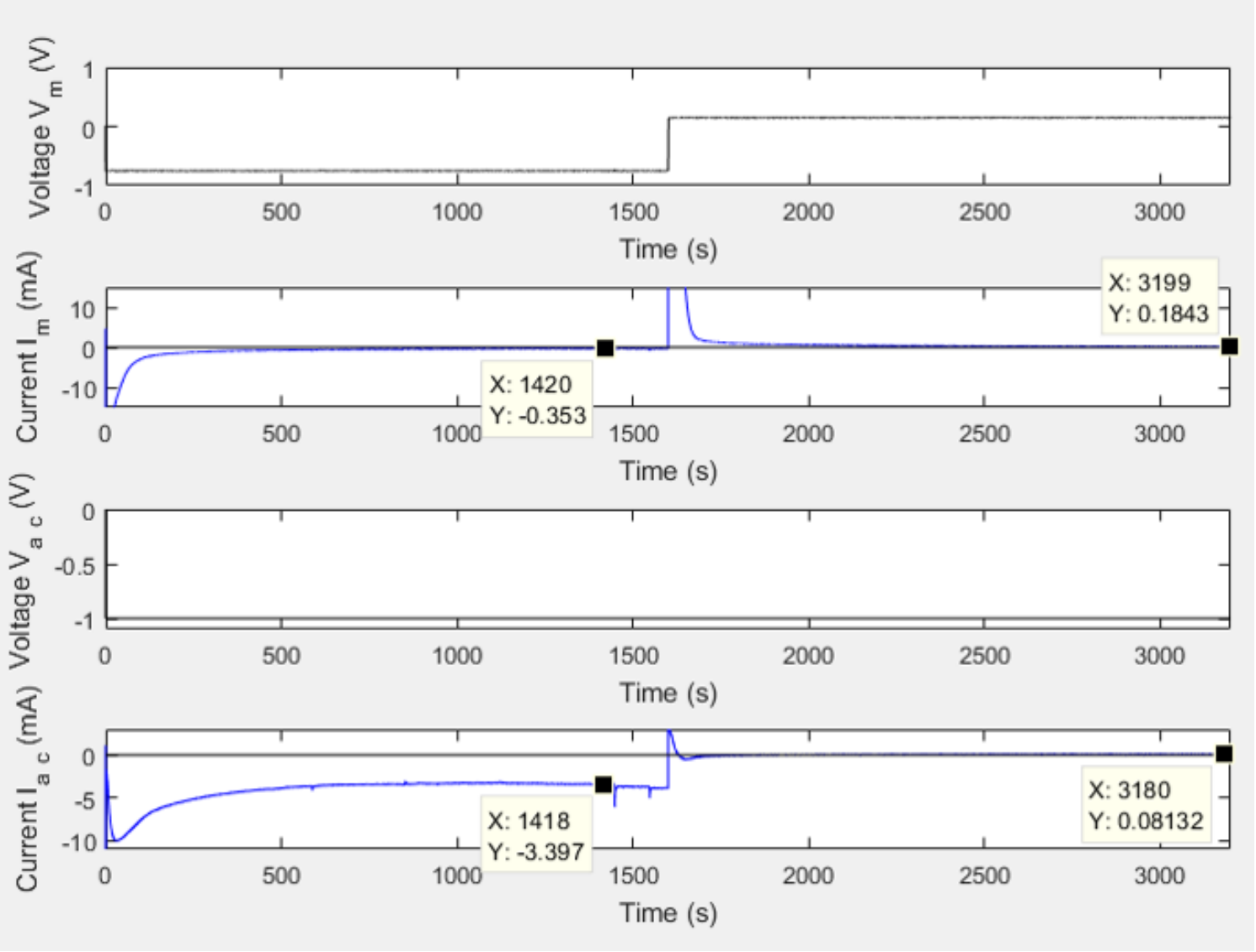

Figure 35: Flow Cell Forced Charge Test 1

The difference between attempted charging in the reduced and oxidized phases is quite clear in this test. The steady state reduction current levels out around -3.4 mA, while the oxidation current quickly converges to 0.08 mA, which is a significant departure from the reduced current magnitude. I_m currents during this interval reach steady states of roughly -0.4 and 0.2 mA respectively. Some fraction of these I_m values may be attributed to interplay current I_{ma}, but it can be considered small enough to effectively ignore.

To verify these results, the transmembrane test from Figure 31 was applied to the flow cell, then the forced discharge test was conducted again (Figure 36).

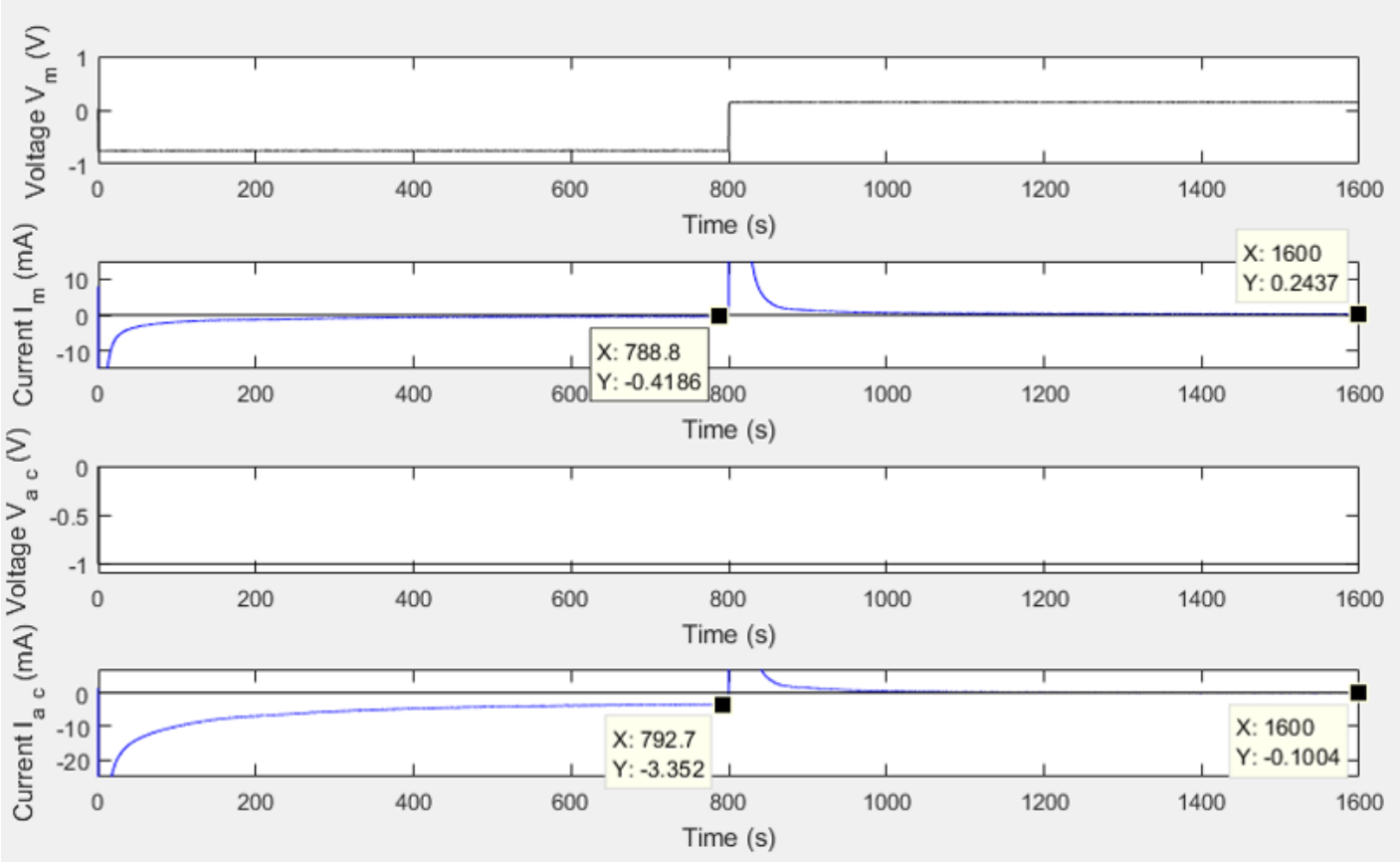

Figure 36: Flow Cell Forced Charge Test 2

The second test results are consistent with the first, as the reduced current reaches a steady state of -3.5 mA, and the oxidized current quickly converges to roughly -0.1 mA.

Membrane current I_m reaches reduced and oxidized current values of -0.4 mA and 0.24 mA respectively. These tests provide initial evidence of the large membrane's ability to limit self-discharge effectively in the oxidized redox state while allowing transmembrane ion transport in the reduced state.

While the membrane appears to exhibit control over leakage current in the oxidized state, it is unclear how the reduced steady state current is affected due to the combined factors of the membrane and the additional Celgard layers. To distinguish between these factors, a forced charge test was conducted using only three plain Celgard separators, shown in Figure 37.

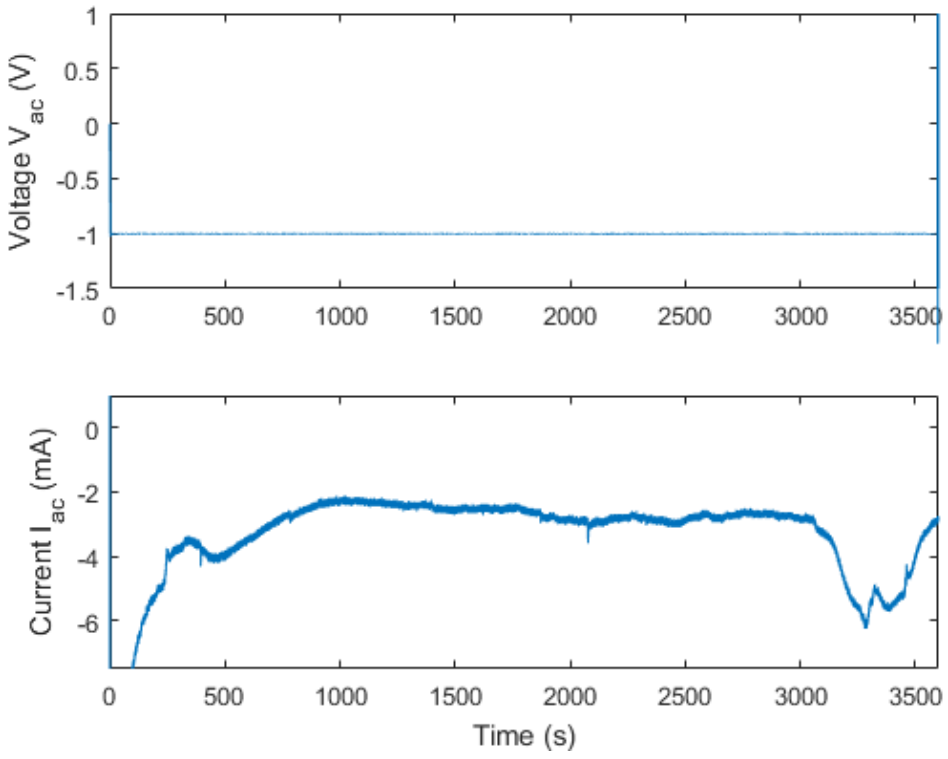

Figure 37: Large Forced Charge with 3 Celgard Layers and no PPy(DBS) membrane

The current data from this test fluctuated slightly over time, but the range over 1000 to 3000 seconds reached a rough steady state of around -2-2.5 mA. These values are lower than

those of the reduced membrane state, indicating that the conducting polymer component of the membrane does not add significant resistance to the mean paths the ions travel across, but may actually aid ion transport through to the applied potential associated with the reduced state. In addition, the oxidized membrane steady state current values are much lower than the baseline current values found through this test. This difference indicates that the polymer in its oxidized state contributes significantly to the resistance across the membrane, and far more than resistances due to the Celgard separators themselves.

Chapter 4: Conclusion

4.1 Contributions

The purpose of this research was to investigate the use of ionic redox transistor membranes in super-capacitive cells. Previous research had shown that the membrane could be used successfully as a transistive element in an electrolytic cell (Hery, 2016), but no testing had been done to characterize the leakage currents associated with the membranes redox states. This study has obtained quantizable evidence of the membrane's ability to drastically reduce leakage current in the oxidized state, while allowing ion transport in the reduced state. In addition, only small-scale samples of the membrane had been used in experiment before this research was conducted, leading to uncertainty about the smart membrane's performance on larger scales. This study has determined that larger membrane sizes are able to be fabricated with improved ion transport characteristics that retain the same general behavior as the smaller samples. The novel fabrication techniques for large membranes that were developed as a part of this study can be translated to smart membrane manufacturing on an industrial scale.

4.2 Limitations and Shortcomings

Many of the tests conducted on the membrane, including the transmembrane and forced charge tests, created non-ideal environments in the cell that a typical super-capacitor membrane in commercial operation would not experience. Situations where the cell is charged or discharged while the membrane is in an oxidized state create a better understanding of how the membrane behaves in a worst-case scenario, but negatively impacts the membrane performance over time. To this extent, we noted in section 3.5 that membrane CV's taken before and after several iterations of forced charge tests indicated significant degradation of

the membrane composition. Whether this decrease in capacity would have occurred in tests operating within ideal conditions is unclear.

Many of the initial tests involving the large flow cell were unsuccessful due to the hydrophobic nature of the unmodified Celgard separators. Though a proper methodology involving soaking separators before assembly was eventually developed, only a few transistor membranes within the flow cell were able to be tested during the back-end of the research period. These membranes demonstrated significant control over ionic currents in the oxidized state, but due to the lack of a large data set, we cannot conclusively state with confidence what factor of reduction the membrane exhibits between steady state reduced and oxidized leakage currents. The forced charge tests shown in this paper display reduction factors of 70 and 10, which vary significantly. More tests must be conducted to provide a probable confidence interval for this reduction factor.

4.3 Recommendations on Future Work

Tests within this study have demonstrate the performance of the membrane within semi-aqueous chemistries. Ethylene glycol was added to solution to simulate a somewhat non-aqueous solution as previous tests had shown membrane ability in aqueous electrolytes. Due to the success of tests presented in this paper, performance of transistor membranes must next be evaluated in non-aqueous electrolyte, as these chemistries allow a wider applied potential range and are far more energy dense. Commercial applications of the transistor membrane, especially in a redox flow cell, will most definitely incorporate non-aqueous electrolyte into the design.

As mentioned in section 4.2, it is unclear whether or not the membrane experiences notable capacity fade when operating under ideal charge-discharge conditions. It is the recommendation of this report that future tests of the transistor membrane constrain it to be reduced while charging and discharging, and only oxidized while little to no transmembrane potential is applied. Aderence to these constraints will better characterize the cyclability of the membrane over time.

Finally, the forced charge test, though destructive, should be iterated more times to determine a confidence interval for the reduction factor between the reduced and oxidized steady state currents. Due to the significance of diminishing leakage current in EES devices, a well-formed understanding of this factor will generate interest in including these transistor membrane components in large-scale batteries and super-capacitors.

Bibliography

1. Duduta, M., Ho, B., Wood, V. C., Limthongkul, P., Brunini, V. E., Carter, W. C. and Chiang, Y.-M. 2011. *Semi-Solid Lithium Rechargeable Flow Battery*. Adv. Energy Mater., 1: 511–516.

2. Gyuk, I. et al. 2013. *Grid Energy Storage*; U.S. Department of Energy, Office of Electricity Delivery & Energy Reliability: Washington, DC, 2013.

3. Glynn, Patrick. 2015. *Preventing Laptop Fires and "Thermal Runaway"*; U.S. DOE Office of Science (SC). N.p, Web, https://science.energy.gov/news/featured-articles/2012/127035/.

4. Hery, T., Sundaresan, V. 2016. *Ionic redox transistor from pore-spanning PPy(DBS) membranes*; Energy Environ. Sci., 2016, 9, 2555-2562

5. J. Niu, B.E. Conway, W.G. Pell. J. Power Sources, 135 (2004), p. 332

6. Soloveichik GL. 2015. *Flow Batteries: Current Status and Trends.* Chem Rev.; 115(20):11533-58.

7. U.S. Energy Information Administration. 2017. *Annual Energy Outlook;* U.S. Department of Energy: Washington, DC.

8. U.S. Energy Information Administration. 2017. *Electric Power Monthly;* U.S. Department of Energy: Washington, DC,

9. Venugopal, V., Sundaresan, V. 2015. *Polypyrrole-based amperometric cation sensor with tunable sensitivity*. J. Int. Mat. Sys., 1-8.

10. Zhang, X. *Biaxially oriented porous membranes, composites, and methods of manufacture and use*. U.S. Patent 20110223486, 2011.